J. Fluid Mech. (2023), *vol*. 961, A28, doi:10.1017/jfm.2023.223

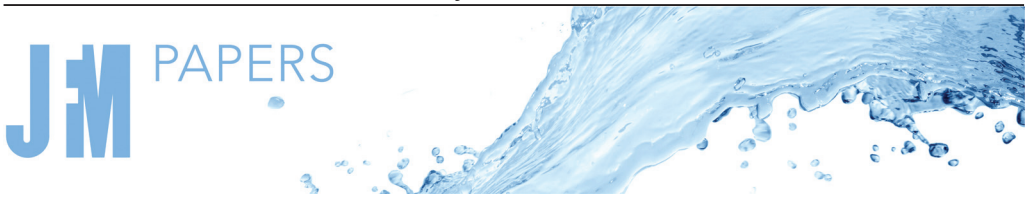

Equilibrium shapes of liquid drops on pre-stretched nonlinear elastic membranes

Vineet Nair[1,2,†], **Ishan Sharma**[1,2,3] **and V. Shankar**[4]

[1]Mechanics & Applied Mathematics Group, Indian Institute of Technology Kanpur, Kanpur 208016, India

[2]Department of Mechanical Engineering, Indian Institute of Technology Kanpur, Kanpur 208016, India

[3]Department of Space Science & Astronomy, Indian Institute of Technology Kanpur, Kanpur 208016, India

[4]Department of Chemical Engineering, Indian Institute of Technology Kanpur, Kanpur 208016, India

(Received 30 January 2022; revised 19 February 2023; accepted 25 February 2023)

We investigate the equilibrium of an axisymmetric system consisting of sessile and pendent drops on pre-stretched nonlinear elastic membranes. The membrane experiences large deformations due to the drop's weight and interfacial interactions. We first show that force balance alone leads to non-unique equilibrium solutions. Identifying the system's equilibrium with the minimum of its free energy, we then demonstrate that the equilibrium solution is made unique by requiring the continuity of meridional stretches across the three-phase contact circle. For a special class of nonlinear elastic materials – I_2 materials – we then compute the equilibrium configurations of the drop–membrane system for a range of drop volumes and membrane pre-tensions. Finally, the present work facilitates two important applications: (a) the membrane's pre-tension and current tension are related exactly to help in utilizing the system as an elastocapillary probe for membrane pre-tension and (b) we suggest an experimental protocol for measuring the membrane's surface properties.

Key words: drops, contact lines, variational methods

1. Introduction

The effect of a sessile liquid drop's surface tension on a deformable solid underneath has long been of interest (Lester 1961; Rusanov 1975). Although most investigations have focused on drops placed upon thick elastic substrates (Style *et al.* 2017; Andreotti & Snoeijer 2020), systems comprising drops on compliant geometries, such as free-standing elastic structures, are being increasingly studied. This is because such systems, through their slenderness, admit easily measurable large deformations, thereby allowing us to

† Email address for correspondence: vnair@iitk.ac.in

determine solid surface energies (Nadermann, Hui & Jagota 2013). The interaction of thin structures with drops has also been studied in the context of other applications and phenomena, such as the design of engineered microstructures, micropatterning and collapse of tubular structures like bronchial airways (Roman & Bico 2010; Bico *et al.* 2018; Paulsen 2019).

Fortes (1984) and Shanahan (1985) were among the first to study the problem of wetting of thin plates and membranes. The former employed the balance of forces, while the latter followed an energy approach to study the deformation of a thin solid by a drop's presence. Shanahan (1985) reported that the contact angle, unlike for a rigid substrate, is not an intrinsic property of the system and depends on the drop's volume and the elastic properties of the solid, in addition to the surface properties of the different phases involved. Shanahan (1987) then investigated the effect of the plate's thickness on the contact angle in the limit of small drops. Additionally, he carried out a semi-quantitative analysis to reveal that an axisymmetric configuration may not be the most stable one.

Olives (1993, 1996) extended the work of Shanahan (1987) by incorporating the contributions of the plate's stretch, but ignored its pre-tension. He obtained the governing equations by minimizing the total free energy of the system comprising of all the surface energies, the drop's gravitational potential and the plate's elastic energy due to contributions from both in-plane stretch and bending. He reported that some components of the displacement gradient at the contact line were discontinuous, in contrast to what had been previously assumed (Kern & Müller 1992), and that the Young–Dupré law, which determines the equilibrium contact angle for liquid drops on rigid substrates, does not hold for liquid drops on thin elastic plates, in contrast to what was reported in Shanahan (1985). Schroll *et al.* (2013) and Davidovitch & Vella (2018) employed the ideas of Olives (1993, 1996) to, respectively, investigate the onset of wrinkling in floating thin elastic sheets when a liquid drop is placed upon them and to include pre-tension of the thin sheet into the theory through a perturbative approach.

The analyses of Olives (1993, 1996), Schroll *et al.* (2013) and Davidovitch & Vella (2018) all employed a Föppl–von Kármán model for a thin film with some variations. In general, the Föppl–von Kármán model is restricted to linear elastic materials and admits only small strains and moderate rotations up to 10°–15° (Reddy, 2006, p. 98). Additionally, Schroll *et al.* (2013) and Davidovitch & Vella (2018) ignored bending resistance, while the latter further specialized their work to nearly inextensible films. At the same time, experiments in Schulman & Dalnoki-Veress (2015) report that rotations may be as large as 40°, while we will later show that strains may also be as much as 15 % for practically relevant system parameters. This motivates us to pursue a model for elastocapillary systems that incorporates the large deformation and nonlinear material response of the thin solid.

Nadermann *et al.* (2013) performed experiments employing different liquid drops hung from stretched free-standing, thin, elastomeric films, and measured solid surface tensions. Schulman & Dalnoki-Veress (2015) experimentally estimated the global contact angles of micro-drops placed upon thin elastomeric and glassy free-standing films. The angles were measured as a function of the tension in the film and were reported to be in agreement with the Neumann construction, which involves a balance of forces at the contact line (de Gennes, Brochard-Wyart & Quéré 2004). Schulman *et al.* (2017) proposed a role of liquid drops as non-destructive probes in determining the stress field in a membrane. However, Davidovitch & Vella (2018) showed that, irrespective of the size of the drop, the tension in the membrane, especially in the vicinity of the contact line, experiences a significant deviation from the uniform, isotropic pre-tension in the membrane prior to the

drop's placement. Thus, in order for drops to be employed as elastocapillary probes for membrane tension, it is necessary to incorporate the nonlinear response and large deformation of a solid in the modelling framework.

Recently, Liu *et al.* (2020) included strain-dependent surface stresses, namely the Shuttleworth effect (Shuttleworth 1950), to analyse the deformations induced by a sessile drop on a nonlinear elastic membrane through a variational formulation. Although they implemented a large-deformation theory, they ignored the role played by the pre-tension in the membrane and the effect of gravity. They specialized their analysis to small spherical drops, so that the drop pressure was constant everywhere, while the dry part of the membrane remained flat. In the absence of the Shuttleworth effect, Liu *et al.* (2020) showed that the meridional stretches are continuous at the triple point where the drop meets the membrane. This condition was previously reported for the planar case by Neukirch, Antkowiak & Marigo (2014) and Hui & Jagota (2015).

In passing we also mention investigations into two-dimensional systems. The planar equilibrium of drops on thin structures was studied by Nair, Sharma & Shankar (2018), who characterized the effect of volume on the global features of the drop–membrane system, by Hui & Jagota (2015), who employed it to elaborate the difference between solid surface energy and solid surface tension, and by Neukirch, Antkowiak & Marigo (2013) and Neukirch *et al.* (2014), who computed the direction of the external force on a beam exerted by the liquid–vapour phase in the absence and presence of extensional deformations. Neukirch *et al.* (2013, 2014) and Nair *et al.* (2018) took the solid structures to be made of linear elastic material but accommodated large rotations, but Hui & Jagota (2015) employed a neo-Hookean material model.

Here, we investigate the axisymmetric system of liquid drops placed upon (sessile drops) or hanging under (pendent drops) pre-stretched, nonlinear elastic circular membranes. We formulate and solve the problem under the assumption of equibiaxial tension and provide a closed-form expression for membrane pre-tension. The constitutive law that allows for such an assumption is also discussed. We show that the solution to the governing equations obtained from a balance of forces alone leads to non-unique equilibrium shapes for fixed system parameters. The necessary condition for uniqueness is obtained by minimizing the free energy of the system, and relates to the continuity of meridional stretches across the three-phase contact circle. Subsequently, we investigate the system's global characteristics, such as the tension distribution in the membrane and the geometry of the drop–membrane system in the vicinity of the three-phase contact line, and their dependence upon on the drop's volume and the membrane's pre-tension. In particular, we provide a closed-form expression for the membrane pre-tension in terms of its tensions when the drop–membrane system equilibrates. This provides the necessary modelling framework for the development of elastocapillary tension probes. Finally, we investigate the effect of the membrane's surface properties and show that they lead to measurable changes in the equilibrium configuration. This suggests a way towards extracting solid surface properties from elastocapillary experiments. In the process we make contact with the recent experiments of Kumar *et al.* (2020) and interpret their results in the context of our modelling approach.

The outline of this paper is as follows. In §§ 2 and 3, we formulate the mathematical model of the system by describing the governing equations and the boundary conditions. We demonstrate the non-uniqueness of the solutions obtained in § 4. In § 5, we reformulate the problem as a minimization of the total free energy of the system and find the necessary condition which ensures uniqueness of the equilibrium solution. This is followed by results and discussion in § 6 and conclusions in § 7.

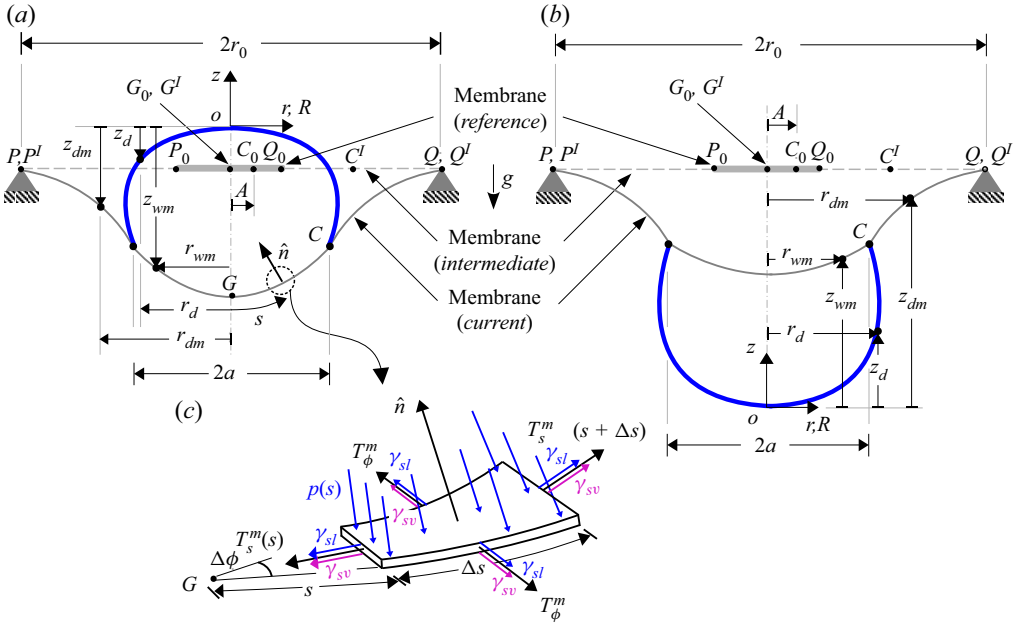

Figure 1. Schematic of a pre-stretched, circular membrane (grey) with (*a*) a sessile drop (blue) and (*b*) a pendent drop (blue) at equilibrium. The reference (unstretched), intermediate (pre-stretched) and current (equilibrium) configurations of the membrane are also shown. (*c*) Free-body diagram of a membrane element at equilibrium with normal $\hat{\boldsymbol{n}}$, mechanical tension T_i^m $(i = s, \phi)$ and membrane–air (γ_{sv}) and membrane–liquid (γ_{sl}) surface tensions indicated. See main text for details.

2. Mathematical model

Here we obtain the governing equations from a consideration of the system's mechanical equilibrium. The reader interested in the variational approach and results may go directly to § 5. Figure 1 depicts schematically the equilibrium configurations of sessile and pendent systems. In these a sessile (pendent) liquid drop is placed upon (hanging under) a pre-stretched, circular membrane that has been clamped along its circumference at a circular boundary of radius r_0.

We assume that the membrane is chemically homogeneous and has a smooth surface. We model the membrane material as a homogeneous, isotropic, incompressible, hyperelastic material (Green & Adkins 1960, p. 148). A hyperelastic material is an elastic material for which there exists a strain energy function (Ogden 1997, p. 206) that relates the stress and strain fields. We admit large deformations of the membrane, and so distinguish between the membrane's reference, intermediate and current configurations, which we now define.

In its reference configuration, for both sessile and pendent systems in figure 1, the membrane is flat and force free. This is indicated in figure 1 by a thick horizontal grey line, on which we have indicated a few representative material points: P_0, G_0, C_0 and Q_0. The membrane is then stretched uniformly and isotropically in its own plane by a stretch ratio $\lambda_0 > 1$ and clamped along the circular boundary, as shown in figure 1 by a dashed horizontal line connecting the two supports. The material points previously at P_0, Q_0, G_0 and C_0 now occupy positions at P^I, Q^I, G^I and C^I, with G^I coinciding with G_0 as the membrane's centre does not move when stretched uniformly. At this stage, the membrane is supposed to be in its intermediate configuration. A drop is then placed at

or hung from the centre of the stretched flat membrane, so that the membrane deforms under the combined action of drop's weight and solid and fluid surface tensions, and finally achieves equilibrium. The equilibrated shape of the membrane is denoted by a solid line, and we label this as the membrane's current configuration. The material points we were following now lie at P, Q, G and C in figure 1. Note that P and Q coincide with their locations in the intermediate configuration as the membrane was pinned. Finally, the material point at C lies on the three-phase contact line where the drop first meets the membrane. This material point, during the course of the membrane's deformation, went from its reference (unstretched membrane) location at C_0 to its intermediate (pre-stretched membrane) location C^I before arriving its current (equilibrium) location at C.

The coordinate systems employed are shown in figure 1. The origin O always lies at the drop's apex. As is standard in large-deformation elasticity, we locate material points in the reference and current configurations through different sets of coordinates, in our case the radial coordinates R and r, respectively. Thus, the material point at C in figure 1 is located at $r = a$, while in the reference configuration the same material point was at $R = A$. In general, if a material point is at the radial location r, then in the reference configuration it lay at a distance R. Note that for the drop only the current configuration is relevant.

2.1. *Governing equations*

We derive the equations governing the equilibrium of the drop and the membrane in turn, considering sessile and pendent systems depicted in figure 1 simultaneously. We restrict ourselves to axisymmetric systems.

In figure 1 the membrane at equilibrium spans $0 \leq r \leq r_0$, with r being the radial coordinate. At equilibrium, the three-phase contact line forms a contact circle of radius a. This allows us to divide the membrane into two parts: the wet and dry membranes that lie between, respectively, $0 \leq r_{wm} \leq a$ and $a \leq r_{dm} \leq r_0$. In the unstretched (reference) state, the wet and dry parts of the membrane occupied, respectively, $0 \leq R_{wm} \leq A$ and $A \leq R_{dm} \leq R_0$, where the radial coordinates R_{wm}, R_{dm} and R_0 locate in the reference configuration material points currently at r_{wm}, r_{dm} and r_0, respectively (see figure 1).

The equation governing the equilibrated shapes of drops is obtained from the Young–Laplace equation and is given by (Bashforth & Adams 1883)

$$\frac{z_d''}{(1+z_d'^2)^{3/2}} + \frac{1}{r_d}\frac{z_d'}{(1+z_d'^2)^{1/2}} = j\left(-\frac{2}{b} + \frac{\rho g z_d}{\gamma}\right), \tag{2.1}$$

where $j = \pm 1$ for sessile/pendent drops, $z_d(r_d)$ is the profile of the drop in figure 1, prime ($'$) always denotes differentiation with respect to relevant radial coordinate, in this case r_d, ρ is the density of the liquid, γ is the liquid–air surface tension, b is the radius of curvature at the apex of the drop and g is the acceleration due to gravity. Both ρ and γ are taken to be uniform. Every solution to (2.1) must satisfy the initial conditions

$$z_d = 0 \quad \text{and} \quad z_d' = 0 \quad \text{at } r_d = 0, \tag{2.2a,b}$$

which follow from our definition of the coordinate system, and axisymmetry of the drop along with its smooth profile. While Bashforth & Adams (1883) obtained (2.1) and (2.2) to describe axisymmetric drops on a rigid surface, the formulation is agnostic to the type of substrate as long as it permits axisymmetric solutions. Finally, the triple point where the three-phase contact line penetrates the rz plane lies at $\{a,\ z_d(a)\}$.

We now consider the equilibrium of the membrane. Because the membrane deforms axisymmetrically, the principal stresses and stretches in the current configuration are in

the meridional (along the arc length s), circumferential (along the azimuthal angle ϕ) and normal (along the unit normal $\hat{n}$) directions of a deformed membrane element (see figure 1 c). Referring to figure 1(c), the balances of forces along the meridional and circumferential directions of a membrane element in the current configuration are (Green & Adkins 1960, p. 151)

$$T_s' + \frac{T_s - T_\phi}{r} = 0 \quad \text{and} \quad \kappa_s T_s + \kappa_\phi T_\phi = \tilde{p}, \tag{2.3a,b}$$

respectively, where $T_s(s)$ and $T_\phi(s)$ are the total principal tensions per unit edge length along the s and ϕ directions, respectively, prime ($'$) now denotes differentiation with respect to the radial coordinate r, $\tilde{p}$ is the normal pressure acting on a membrane element and

$$\kappa_s = \frac{z''}{(1+z'^2)^{3/2}} \quad \text{and} \quad \kappa_\phi = \frac{1}{r}\frac{z'}{(1+z'^2)^{1/2}} \tag{2.4a,b}$$

are principal curvatures along the s and ϕ directions (Kühnel 2015, p. 95), where $z(r)$ describes the membrane's equilibrium (current) profile in the rz plane. The normal pressure

$$\tilde{p} = -j\left(\frac{-2\gamma}{b} + \rho g z\right) \tag{2.5}$$

is the pressure exerted on the membrane by a fluid column in the drop and has contributions from both the Laplace pressure and the liquid's weight. We emphasize that the total principal tensions $T_s(s)$ and $T_\phi(s)$ are the sum of the mechanical tension in the membrane and the surface tensions associated with the membrane–liquid and membrane–air interfaces (see the derivation in Appendix A). The mechanical tension is really the internal or Cauchy tension in the membrane that arises from the action of one part of the membrane on the other across a dividing surface (see Love 1927, Note B).

To complete the description of the membrane's deformation we need to relate the tensions in the membrane to the stretch it experiences. In a hyperelastic membrane the principal mechanical tensions may be obtained in terms of a strain energy density function W (Green & Adkins 1960; Haughton 2001) so that, following Long, Shull & Hui (2010), we may write

$$T_s = \frac{t_0}{\hat{\lambda}_\phi}\frac{\partial W}{\partial \hat{\lambda}_s} + \gamma_m \quad \text{and} \quad T_\phi = \frac{t_0}{\hat{\lambda}_s}\frac{\partial W}{\partial \hat{\lambda}_\phi} + \gamma_m, \tag{2.6a,b}$$

where t_0 is the thickness of the membrane in the reference configuration, $\hat{\lambda}_s$ and $\hat{\lambda}_\phi$ are the total principal stretches with respect to the reference configuration in the s and ϕ directions, respectively, and γ_m is the membrane surface tension that is assumed to be uniform and isotropic. Equation (2.6) expresses in mathematical terms the split of the total tension in terms of the mechanical tension and the surface tensions mentioned above. For an isotropic, incompressible and hyperelastic material, the strain energy density function has the following form (Ogden 1997, p. 220):

$$W = W(I_1, I_2), \tag{2.7}$$

where I_1 and I_2 are, respectively, the first and second principal invariants of the Cauchy–Green deformation tensor $\boldsymbol{F}\boldsymbol{F}^T$, with $\boldsymbol{F}$ being the deformation gradient (Ogden 1997, p. 218) of the material. The principal invariants for the membrane may be expressed in terms of its principal stretches by

$$I_1 = \hat{\lambda}_s^2 + \hat{\lambda}_\phi^2 + (\hat{\lambda}_s\hat{\lambda}_\phi)^{-2} \quad \text{and} \quad I_2 = \hat{\lambda}_s^{-2} + \hat{\lambda}_\phi^{-2} + (\hat{\lambda}_s\hat{\lambda}_\phi)^2, \tag{2.8a,b}$$

where the principal stretch along unit normal $\hat{n}$ is set to $(\hat{\lambda}_s\hat{\lambda}_\phi)^{-1}$ in order to satisfy the incompressibility condition. The principal stretches $\hat{\lambda}_s$ and $\hat{\lambda}_\phi$ are, in turn, given by

$$\hat{\lambda}_s = \lambda_0\lambda_s = \lambda_0 \left\{ \left(\frac{\mathrm{d}r}{\mathrm{d}R^I} \right)^2 + \left(\frac{\mathrm{d}z}{\mathrm{d}R^I} \right)^2 \right\}^{1/2} \tag{2.9a}$$

and

$$\hat{\lambda}_\phi = \lambda_0\lambda_\phi = \lambda_0 r/R^I, \tag{2.9b}$$

where λ_0, we recall, is the uniform, in-plane, isotropic stretch relating the reference to the intermediate configuration in figure 1, R^I is the radial coordinate in the intermediate configuration of a material point of the membrane currently at r and

$$\lambda_s = \sqrt{(\mathrm{d}r/\mathrm{d}R^I)^2 + (\mathrm{d}z/\mathrm{d}R^I)^2} \quad \text{and} \quad \lambda_\phi = r/R^I \tag{2.10a,b}$$

are principal stretches in the meridional and circumferential directions, respectively, that relate the membrane's intermediate and current configurations.

Now, when the stretches in the membrane are large, i.e. $\hat{\lambda}_s, \hat{\lambda}_\phi \gg 1$, we have $I_1 \approx \hat{\lambda}_s^2 + \hat{\lambda}_\phi^2$ and $I_2 \approx (\hat{\lambda}_s\hat{\lambda}_\phi)^2$ and, thus, $I_2 \gg I_1$. Under such circumstances, we proceed by retaining the dependence of W on I_2 alone. Then, following Long & Hui (2012), we restrict ourselves to a class of hyperelastic membranes with $W = \hat{W}(I_2)$, henceforth called membranes made of I_2 materials, or I_2 membranes for brevity.

The principal tensions (2.6) become equal in membranes with I_2 materials, i.e.

$$T_s = T_\phi = 2t_0\hat{\lambda}_s\hat{\lambda}_\phi \frac{\mathrm{d}\hat{W}}{\mathrm{d}I_2} + \gamma_m =: T; \tag{2.11}$$

thus, under large stretches the membrane experiences an equibiaxial tension given by $T(s)$. Such a scenario may arise when the pre-stretch $\lambda_0 \gg 1$ or drop volumes are moderate/large. In the latter case, the effect of gravity must be considered. With the membrane under equibiaxial tension (2.11), the force balance along the meridional direction (2.3*a*) provides

$$T = 2t_0\hat{\lambda}_s\hat{\lambda}_\phi \frac{\partial\hat{W}}{\partial I_2} + \gamma_m = \text{constant}, \tag{2.12}$$

i.e. the tension T in the membrane is uniform. This also suggests that the product of the principal stretches is the same everywhere, although the individual stretches need not be uniform (Long & Hui 2012). We note that the choice of I_2 membranes is a simplifying but not a limiting assumption. The present framework has been utilized to investigate a wider class of non-Hookean membranes (Nair 2022) in which $T_s \neq T_\phi$.

We now adapt the above derivation to the equilibrium of wet and dry membranes in the presence of a drop, as in figure 1. Combining (2.5), (2.4) and (2.11), the force balance along the normal direction (2.3*b*) yields the equation governing the profiles of the wet

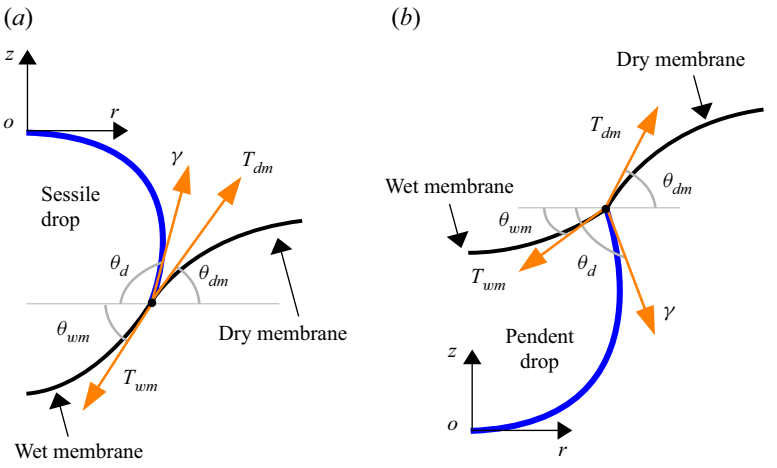

Figure 2. Local geometry and the forces acting at the triple point of a membrane at equilibrium with (*a*) a sessile drop and (*b*) a pendent drop.

(z_{wm}) and dry membranes (z_{dm}) as, respectively,

$$T_{wm}\left\{\frac{z''_{wm}}{(1+z'^2_{wm})^{3/2}}+\frac{1}{r_{wm}}\frac{z'_{wm}}{(1+z'^2_{wm})^{1/2}}\right\}=-j\left(-\frac{2\gamma}{b}+\rho g z_{wm}\right) \tag{2.13}$$

and

$$T_{dm}\left\{\frac{z''_{dm}}{(1+z'^2_{dm})^{3/2}}+\frac{1}{r_{dm}}\frac{z'_{dm}}{(1+z'^2_{dm})^{1/2}}\right\}=0, \tag{2.14}$$

where T_{wm} and T_{dm} are the uniform, equibiaxial tensions in the wet and dry membranes. To obtain (2.14), we have utilized the fact that the dry membrane is free from external loads.

Before we specify the boundary conditions, we will establish the local geometry at the triple point and the forces acting there, as displayed in figure 2. Balance of forces along the r and z directions provides, in turn,

$$T_{dm}\cos\theta_{dm}-\gamma\cos\theta_d-T_{wm}\cos\theta_{wm}=0 \tag{2.15a}$$

and

$$T_{dm}\sin\theta_{dm}+j\gamma\sin\theta_d-T_{wm}\sin\theta_{wm}=0, \tag{2.15b}$$

where the drop angle θ_d, the wet membrane angle θ_{wm} and the dry membrane angle θ_{dm} are the angles made at the triple point with the horizontal by the drop, the wet membrane and the dry membrane, respectively. The drop angle θ_d is also sometimes referred to as the apparent contact angle in the literature (Liu *et al.* 2020). We note that (2.15) is analogous to Neumann's triangle involving the balance of surface tensions in a system consisting of three fluid phases (de Gennes *et al.* 2004).

We may now write the boundary conditions for the wet membrane as

$$z'_{wm} = 0 \text{ at } r_{wm} = 0 \quad \text{and} \quad z_{wm} = z_d \text{ at } r_{wm} = a, \tag{2.16a,b}$$

where the latter follows from the membrane's profile $z_{wm}(r_{wm})$ in the rz plane passing through the triple point $\{a,\ z_d(a)\}$. The boundary conditions for the dry membrane are

$$z_{dm} = z_d \quad \text{and} \quad z'_{dm} = \tan\theta_{dm} \quad \text{at } r_{dm} = a. \tag{2.17a,b}$$

This completes the formulation of the drop–membrane system based purely upon balance of forces. At present, the interfacial interaction was modelled through surface tension forces, and we will revisit this in § 5. Note also that the drop's volume is computed after solving for the equilibrium shapes of the drop and the membrane, and is not an *a priori* constraint imposed upon the system.

2.2. *Non-dimensionalization*

We now non-dimensionalize the governing equations. We set

$$r_d/r_0 = \bar{r}_d, \quad z_d/r_0 = \bar{z}_d, \quad a/r_0 = \bar{a} \quad \text{and} \quad b/r_0 = \bar{b}, \tag{2.18a–d}$$

where r_0 is the radius of the clamped boundary (see figure 1). With this (2.1) and (2.2) become

$$\frac{\bar{z}''_d}{(1+\bar{z}'^2_d)^{3/2}} + \frac{1}{\bar{r}_d}\frac{\bar{z}'_d}{(1+\bar{z}'^2_d)^{1/2}} = j(-2\beta + \omega^2\bar{z}_d) \tag{2.19}$$

and

$$\bar{z}_d = 0 \quad \text{and} \quad \bar{z}'_d = 0 \quad \text{at } \bar{r}_d = 0, \tag{2.20a,b}$$

respectively, where $\beta := 1/b$ is the non-dimensionalized curvature of the drop at its apex and

$$\omega = r_0/l_c, \quad \text{with } l_c = \sqrt{\gamma/\rho g} \tag{2.21}$$

being the capillary length associated with the liquid forming the drop.

We next non-dimensionalize the equations governing the wet and dry membranes. We set

$$r_k/r_0 = \bar{r}_k, \quad z_k/r_0 = \bar{z}_k \quad \text{and} \quad T_k/\gamma = \bar{T}_k, \tag{2.22a–c}$$

where the subscript $k = wm$ or dm, as appropriate, and we recall that γ is the drop's surface tension. Thus, for the wet membrane, (2.13) and (2.16) are non-dimensionalized to obtain

$$\bar{T}_{wm}\left\{\frac{\bar{z}''_{wm}}{(1+\bar{z}'^2_{wm})^{3/2}} + \frac{1}{\bar{r}_{wm}}\frac{\bar{z}'_{wm}}{(1+\bar{z}'^2_{wm})^{1/2}}\right\} = -j(-2\beta + \omega^2\bar{z}_{wm}) \tag{2.23}$$

and

$$\bar{z}'_{wm} = 0 \text{ at } \bar{r}_{wm} = 0 \quad \text{and} \quad \bar{z}_{wm} = \bar{z}_d \quad \text{at } \bar{r}_{wm} = \bar{a}, \tag{2.24a,b}$$

respectively. Similarly, for the dry membrane, (2.14) and (2.17) we find, in turn,

$$\bar{T}_{dm}\left\{\frac{\bar{z}''_{dm}}{(1+\bar{z}'^2_{dm})^{3/2}} + \frac{1}{\bar{r}_{dm}}\frac{\bar{z}'_{dm}}{(1+\bar{z}'^2_{dm})^{1/2}}\right\} = 0 \tag{2.25}$$

and

$$\bar{z}_{dm} = \bar{z}_d \quad \text{and} \quad \bar{z}'_{dm} = \tan\theta_{dm} \quad \text{at } \bar{r}_{dm} = \bar{a}. \tag{2.26a,b}$$

Finally, the balance of forces (2.15) at the triple point is non-dimensionalized to yield

$$\bar{T}_{dm}\cos\theta_{dm} - \cos\theta_d - \bar{T}_{wm}\cos\theta_{wm} = 0 \tag{2.27a}$$

and

$$\bar{T}_{dm}\sin\theta_{dm} + j\sin\theta_d - \bar{T}_{wm}\sin\theta_{wm} = 0. \tag{2.27b}$$

3. Membrane pre-tension

We provide an outline of our solution procedure in Appendix B. It is important to note that the tensions $\bar{T}_{wm}$ and $\bar{T}_{dm}$ in the membrane are related to the system's equilibrium geometry and, so, are independent of the elastic properties of the membrane. The membrane's material affects the amount of pre-stretch that needs to be provided, as we discuss next.

The solution algorithm given in Appendix B finds the system's equilibrium for a choice of apex drop curvature β, contact circle radius $\bar{a}$ and current wet membrane tension $\bar{T}_{wm}$. At the same time, in typical experiments the membrane is stretched and affixed to a boundary prior to the drop's placement. This membrane pre-tension is measurable in experiments and it is expected that the pre-tension should be kept the same in order to compare results across different experiments. We will thus relate the pre-tension to the system's equilibrium configuration, which is again quantifiable in experiments.

To compute the pre-tension we need to select a particular form for the strain energy density function. We employ the Mooney–Rivlin strain energy function (Holzapfel 2000, p. 238):

$$W = \frac{\mu}{2}C_1(I_1 - 3) + \frac{\mu}{2}(1 - C_1)(I_2 - 3), \tag{3.1}$$

where μ is the shear modulus and $0 \le C_1 \le 1$ is a material constant. For reasons listed previously, we focus here upon membranes made of I_2 materials for which $W = \hat{W}(I_2)$, where $I_2 \approx (\hat{\lambda}_s\hat{\lambda}_\phi)^2$. To this end, we set $C_1 = 0$, so that

$$W = \hat{W}(I_2) = \frac{\mu}{2}(I_2 - 3), \tag{3.2}$$

which is the strain energy function that we will utilize.

We now combine the membrane stretches (2.9) with the membrane tension (2.12) and non-dimensionalize to find the non-dimensional tensions in the wet and dry membranes as

$$\bar{T}_{wm} = \alpha_0\lambda_0^2\frac{\bar{r}_{wm}}{\bar{R}^I_{wm}}\sqrt{1 + \bar{z}'^2_{wm}}\frac{\mathrm{d}\bar{r}_{wm}}{\mathrm{d}\bar{R}^I_{wm}} + \bar{\gamma}_{sl} + \bar{\gamma}_{sv} \tag{3.3}$$

and

$$\bar{T}_{dm} = \alpha_0\lambda_0^2\frac{\bar{r}_{dm}}{\bar{R}^I_{dm}}\sqrt{1 + \bar{z}'^2_{dm}}\frac{\mathrm{d}\bar{r}_{dm}}{\mathrm{d}\bar{R}^I_{dm}} + 2\bar{\gamma}_{sv}, \tag{3.4}$$

respectively, where

$$\bar{R}^I_k = R^I_k/r_0 \quad (k = dm, wm), \quad \alpha_0 = \mu t_0/\gamma, \quad \bar{\gamma}_{sl} = \gamma_{sl}/\gamma \quad \text{and} \quad \bar{\gamma}_{sv} = \gamma_{sv}/\gamma, \tag{3.5a–d}$$

with γ_{sl} and γ_{sv} being the surface tensions associated with the membrane–drop and membrane–air interfaces. We recall that the superscript 'I' indicates the intermediate configuration in figure 1. When deriving $\bar{T}_{wm}$ and $\bar{T}_{dm}$ above, we set the membrane

surface tension γ_m in (2.12) equal to $\gamma_{sl}+\gamma_{sv}$ for the wet membrane and $2\gamma_{sv}$ for the dry membrane.

We rewrite (3.3) and integrate both sides:

$$\int_0^{\bar{A}^I} \bar{R}^I_{wm}\,\mathrm{d}\bar{R}^I_{wm} = \frac{\alpha_0\lambda_0^2}{\bar{T}^m_{wm}}\int_0^{\bar{a}} \bar{r}_{wm}\sqrt{1+\bar{z}'^2_{wm}}\,\mathrm{d}\bar{r}_{wm} \tag{3.6}$$

to obtain

$$(\bar{A}^I)^2 = \left(\frac{2\alpha_r\lambda_0^2}{\bar{T}^m_{wm}}\right)\int_0^{\bar{a}} \bar{r}_{wm}\sqrt{1+\bar{z}'^2_{wm}}\,\mathrm{d}\bar{r}_{wm}, \tag{3.7}$$

where $\bar{A}^I = A^I/r_0$ is the location of the triple point $\bar{a}$ in the intermediate configuration, and

$$\bar{T}^m_{wm} = \bar{T}_{wm} - \bar{\gamma}_{sl} - \bar{\gamma}_{sv} \tag{3.8}$$

is the mechanical wet membrane tension. Similarly, we rewrite (3.4) and integrate both sides:

$$\int_{\bar{A}^I}^1 \bar{R}^I_{dm}\,\mathrm{d}\bar{R}^I_{dm} = \frac{\alpha_0\lambda_0^2}{\bar{T}^m_{dm}}\int_{\bar{a}}^1 \bar{r}_{dm}\sqrt{1+\bar{z}'^2_{dm}}\,\mathrm{d}\bar{r}_{dm} \tag{3.9}$$

to find

$$(\bar{A}^I)^2 = 1 - \left(\frac{2\alpha_0\lambda_0^2}{\bar{T}^m_{dm}}\right)\int_{\bar{a}}^1 \bar{r}_{dm}\sqrt{1+\bar{z}'^2_{dm}}\,\mathrm{d}\bar{r}_{dm}, \tag{3.10}$$

where, now,

$$\bar{T}^m_{dm} = \bar{T}_{dm} - 2\bar{\gamma}_{sv} \tag{3.11}$$

is the mechanical dry membrane tension. Because the tensions $\bar{T}_{wm}$ and $\bar{T}_{dm}$ are independent of the membrane's elastic properties, so too are the mechanical tensions. Finally, equating (3.7) and (3.10) we compute the pre-stretch in the membrane to be

$$\lambda_0^2 = \alpha_0^{-1}\left(\frac{2\bar{\Omega}_{wm}}{\bar{T}^m_{wm}} + \frac{2\bar{\Omega}_{dm}}{\bar{T}^m_{dm}}\right)^{-1}, \tag{3.12}$$

where the non-dimensional surface areas of the wet and dry membranes are, respectively,

$$\bar{\Omega}_{wm} = \int_0^{\bar{a}} \bar{r}_{wm}\sqrt{1+\bar{z}'^2_{wm}}\,\mathrm{d}\bar{r}_{wm} \quad \text{and} \quad \bar{\Omega}_{dm} = \int_{\bar{a}}^1 \bar{r}_{dm}\sqrt{1+\bar{z}'^2_{dm}}\,\mathrm{d}\bar{r}_{dm}; \tag{3.13a,b}$$

note that the pre-stretch depends upon the parameter $\alpha_0 = \mu t_0/\gamma$, which is the scaled shear modulus of the membrane.

Now, from the definition (2.6) of a hyperelastic material and the constitutive relation (3.2), the non-dimensional, uniform, isotropic membrane pre-tension T_0 corresponding to

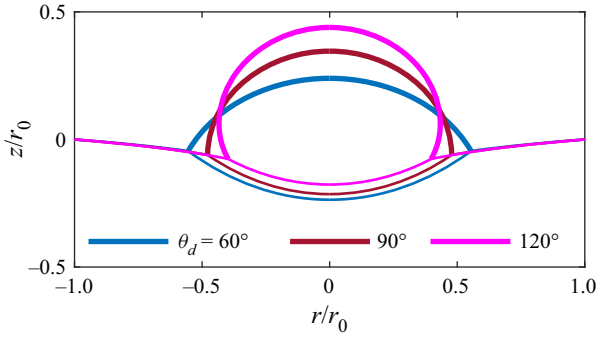

Figure 3. Equilibrium configurations corresponding to three choices of the drop angle θ_d when a sessile drop having non-dimensional volume $\bar{V} = 2$ is placed upon a pre-stretched nonlinear elastic membrane with non-dimensional pre-tension $\bar{T}_0 = 2$. The membrane surface tensions $\bar{\gamma}_{sv} = \bar{\gamma}_{sl} = 0.5$.

a uniform, isotropic pre-stretch $\lambda_0 \gg 1$ is given by

$$\bar{T}_0 = \alpha_0 \lambda_0^2 + 2\bar{\gamma}_{sv}. \tag{3.14}$$

Combining (3.12) with (3.14), we obtain the non-dimensional membrane pre-tension as

$$\bar{T}_0 = \left(\frac{2\bar{\Omega}_{wm}}{\bar{T}^m_{wm}} + \frac{2\bar{\Omega}_{dm}}{\bar{T}^m_{dm}} \right)^{-1} + 2\bar{\gamma}_{sv}. \tag{3.15}$$

We note that the non-dimensional pre-tension $\bar{T}_0$ is also independent of the membrane's shear modulus μ and thickness t_0. As (3.14) shows, the effect of the membrane's properties is expressed through the pre-stretch λ_0.

We end this section with the following remark, which is revisited at the end of § 5. The solution algorithm given in Appendix B indicates that we need to specify three parameters, namely the drop curvature β at its apex, the radius $\bar{a}$ of the contact circle and the wet membrane tension $\bar{T}_{wm}$ at equilibrium, in order to obtain a unique equilibrium configuration. From this the volume of the drop and the pre-tension in the membrane may be computed through (B4) and (3.15), respectively. However, it is more natural and useful to fix the drop's volume $\bar{V}$ and the wet membrane's pre-tension $\bar{T}_0$ when reporting results, and we do this below. Further, as a third parameter we employ the drop angle θ_d, computed in Step I of the solution algorithm in Appendix B, as it is more accessible than the radius $\bar{a}$.

4. Equilibrium configurations: non-uniqueness

We now follow the methodology of the previous section to solve for the equilibrium of a sessile drop on a pre-stretched membrane. Figure 3 shows three possible equilibrium configurations for a given drop volume $\bar{V}$ and membrane pre-tension $\bar{T}_0$, obtained by fixing three values of the drop angle θ_d. Although we display only three equilibria, in fact, there exist infinitely many equilibria, corresponding to every possible choice of θ_d.

Now, in a typical experiment the membrane's pre-tension is first set and a drop of known volume is placed on the membrane. The system then achieves a unique configuration at equilibrium, which entails fixing a particular value of the drop angle θ_d. Thus, it appears that we need one more condition to reduce the choice of the free parameters in our theory to two and force balance alone provides an incomplete description.

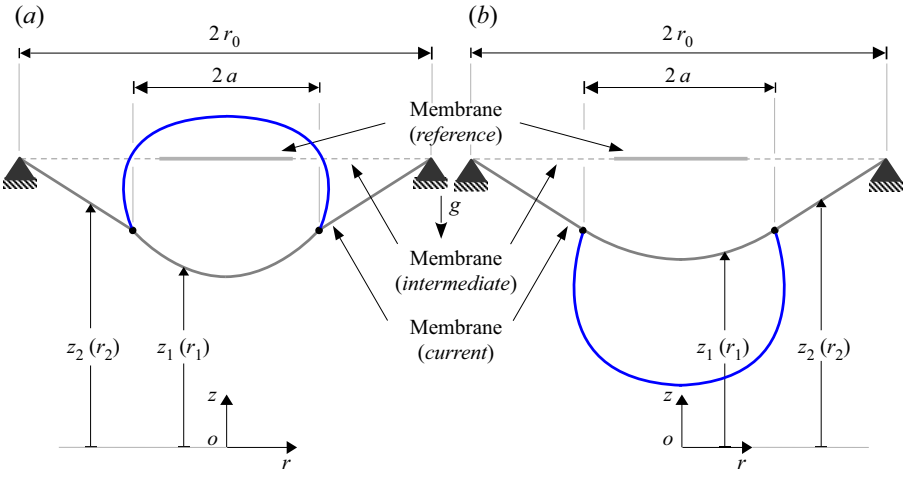

Figure 4. Schematic of axisymmetric drop–membrane systems: (*a*) sessile drop; (*b*) pendent drop. The coordinate system is placed at the datum which is at a fixed distance below the level of the clamp at which the membrane is pinned.

The extra condition that will ensure uniqueness of the equilibrium solution will now be found by minimizing the total free energy of the system. The governing equations obtained above will also be recovered as part of the process.

5. Energy minimization

We expect that the system's equilibrium configuration will minimize the system's total potential energy while keeping the drop volume and the unstretched membrane surface area constant for a given membrane thickness t_0. This is equivalent to the minimizing the Helmholtz free energy – free energy for short – of the mechanical system. Figure 4 shows a schematic of the system we are considering, but now with a coordinate system whose origin is at a fixed distance below the clamp. We revert to a dimensional framework in this section to make the derivation transparent. Quantities without subscript refer to the drop, while those with subscripts '1' and '2' pertain to the wet and dry membranes, respectively. The drop's profile is given by $z = z(r)$, while the profiles of the wet and dry membranes are defined by, respectively, $z_1 = z_1(r_1)$ and $z_2 = z_2(r_2)$. At the same time, with $k = 1$ or 2, we may express the current radial (r_k) and vertical (z_k) locations of a material point in terms of its radial location R_k in the reference configuration as $r_k = \hat{r}_k(R_k)$ and $z_k = \hat{z}_k(R_k)$.

The total potential energy of the system is given by

$$\begin{aligned} E_T = {} & 2\pi\gamma \int_0^a r\sqrt{1+z'^2}\,\mathrm{d}r + j\pi\rho g \int_0^a z^2 r\,\mathrm{d}r - j\pi\rho g \int_0^a z_1^2 r_1\,\mathrm{d}r_1 \\ & + 2\pi \int_0^A \left(R_1 W_1(\hat{\lambda}_{s1}, \hat{\lambda}_{\phi 1}) + (\gamma_{sv} + \gamma_{sl})\hat{r}_1 \sqrt{\hat{r}_1'^2 + \hat{z}_1'^2} \right) \mathrm{d}R_1 \\ & + 2\pi \int_A^{R_0} \left(R_2 W_2(\hat{\lambda}_{s2}, \hat{\lambda}_{\phi 2}) + 2\gamma_{sv}\hat{r}_2 \sqrt{\hat{r}_2'^2 + \hat{z}_2'^2} \right) \mathrm{d}R_2, \end{aligned} \tag{5.1}$$

where we recall that $j = \pm 1$ for sessile/pendent drops, W_k $(k = 1, 2)$ are the strain energy density functions of the wet and dry membranes, $\hat{\lambda}_{sk} = \sqrt{\hat{r}_k'^2 + \hat{z}_k'^2}$ and $\hat{\lambda}_{\phi k} = \hat{r}_k / r_k$ are,

respectively, the total meridional and circumferential stretches, the prime ($'$) denotes differentiation with respect to the independent variable, so that $z' = \mathrm{d}z/\mathrm{d}r$, $\hat{r}_k' = \mathrm{d}\hat{r}_k/\mathrm{d}R_k$ and $\hat{z}_k' = \mathrm{d}\hat{z}_k/\mathrm{d}R_k$, and γ, γ_{sv} and γ_{sl} are the surface energies at the liquid–air, membrane–air and membrane–liquid interfaces, respectively. In (5.1), the first integral is the total surface energy of the drop, the second and third integrals constitute the gravitational potential energy of the drop, while the fourth and fifth integrals include the total strain and surface energies of the wet and dry parts of the membrane, respectively. Note that the membrane's strain energy is defined per unit area of the reference configuration, but the surface energy of the membrane is per unit area of the current configuration. Finally, in (5.1) we have taken the surface energies numerically equal to the surface tensions, and hence employed the same notation. This is a simplifying and commonly employed assumption (Andreotti & Snoeijer 2020). Strain-dependent surface energies may easily be incorporated into our overall process in the manner of, for example, Liu *et al.* (2020).

We wish to minimize E_T while keeping the drop's volume constant at, say, V_0. This is done most expeditiously by considering the augmented functional

$$H_T = E_T + 2\pi p\left(j\int_0^a zr\,\mathrm{d}r - j\int_0^A z_1 r_1\,\mathrm{d}r_1 - V_0\right), \tag{5.2}$$

where p is a Lagrange multiplier, which will turn out to be the thermodynamic pressure. The unstretched membrane's surface area is kept constant by fixing R_0 in (5.1). Note that H_T is the total free energy of the system.

Combining (5.1) and (5.2), rearranging terms and setting $\mathrm{d}r_1 = \hat{r}_1'\,\mathrm{d}R_1$, we obtain

$$\begin{aligned} H_T[z,\hat{r}_1,\hat{z}_1,\hat{r}_2,\hat{z}_2,p] = &\int_0^a (F+pG)\,\mathrm{d}r + \int_0^A (F_1+pG_1)\,\mathrm{d}R_1 \\ &+ \int_A^{R_0} F_2\,\mathrm{d}R_2 - pV_0, \end{aligned} \tag{5.3}$$

where

$$F(r,z,z') = 2\pi\left(\gamma r\sqrt{1+z'^2} + j\frac{\rho g}{2}z^2 r\right), \tag{5.4a}$$

$$G(r,z) = 2\pi jzr, \tag{5.4b}$$

$$F_1(r_1,\hat{r}_1,\hat{z}_1,\hat{r}_1',\hat{z}_1') = 2\pi\left\{R_1W_1 + (\gamma_{sv}+\gamma_{sl})\hat{r}_1\sqrt{\hat{r}_1'^2+\hat{z}_1'^2} - j\frac{\rho g}{2}\hat{z}_1^2\,\hat{r}_1\,\hat{r}_1'\right\}, \tag{5.4c}$$

$$G_1(\hat{r}_1,\hat{z}_1,\hat{r}_1') = -2\pi j\hat{z}_1\,\hat{r}_1\,\hat{r}_1' \tag{5.4d}$$

and

$$F_2(r_2,\hat{r}_2,\hat{r}_2',\hat{z}_2') = 2\pi\left(R_2W_2 + 2\gamma_{sv}\hat{r}_2\sqrt{\hat{r}_2'^2+\hat{z}_2'^2}\right). \tag{5.4e}$$

A necessary condition for the free energy functional H_T to have a minimizer is that the first variation of H_T must vanish due to all admissible perturbations in the fields $z(r)$, $\hat{r}_k(R_k)$ and $\hat{z}_k(R_k)$, with $k = 1, 2$. The end-points $r = r_1 = R_1 = 0$, $r_2 = r_0$ and $R_2 = R_0$ of the system's domain remain fixed. This follows from the system's symmetry, the clamping of the membrane at its edges and because the length of the unstretched membrane is fixed. However, we permit perturbations in the location of the triple point, as well as in the values there of the fields $z(r)$, $\hat{r}_k(R_k)$ and $\hat{z}_k(R_k)$. This acknowledges the fact that the three-phase contact line is determined internally by the system and cannot be externally specified.

We first recall (Gelfand & Fomin 2000, Ch. 3) that a field may be perturbed independently in the interior and at the ends of its domain. Computing the first variation in the five fields $z(r)$, $\hat{r}_k(R_k)$ and $\hat{z}_k(R_k)$ due to perturbations in the interior of the domain leads to a set of five Euler–Lagrange equations. From these equations we exactly recover the governing equations for the drop (2.1) and for the wet and dry membranes (2.13) and (2.14), respectively. The surface energies γ, γ_{sl} and γ_{sv} now appear in the form of surface tensions, consistent with the free-body diagram in figure 1(*c*). The constraint on the volume carries over as is and may be identified with (B4). The details of these calculations may be found in Nair (2022). Variational analysis thus independently confirms the validity of the governing equations (2.13) and (2.14). Moreover, we note that the energy minimization clearly shows the validity of (2.6) with the mechanical equilibrium of the membrane being determined by the total tension T and not just the mechanical part T^m. This is consistent with previous work (Shanahan 1985; Neukirch *et al.* 2014; Liu *et al.* 2020).

Turning to the first variation in H_T obtained from perturbations in the fields at the ends of their domains leads to

$$\begin{aligned}
&\left(\frac{\partial F}{\partial z'}+p\frac{\partial G}{\partial z'}\right)\delta z\Big|_{r=0}^{r=a}+\left(\frac{\partial F_1}{\partial \hat{r}_1'}+p\frac{\partial G_1}{\partial \hat{r}_1'}\right)\delta\hat{r}_1\Big|_{R_1=0}^{R_1=A}+\left(\frac{\partial F_1}{\partial \hat{z}_1'}+p\frac{\partial G_1}{\partial \hat{z}_1'}\right)\delta\hat{z}_1\Big|_{R_1=0}^{R_1=A}\ldots\\
&+\frac{\partial F_2}{\partial \hat{r}_2'}\delta\hat{r}_2\Big|_{R_2=A}^{R_2=R_0}+\frac{\partial F_2}{\partial \hat{z}_2'}\delta\hat{z}_2\Big|_{R_2=A}^{R_2=R_0}+\left\{(F+pG)-\left(\frac{\partial F}{\partial z'}+p\frac{\partial G}{\partial z'}\right)z'\right\}\delta r\Big|_{r=0}^{r=a}\ldots\\
&+\left\{(F_1+pG_1)-\left(\frac{\partial F_1}{\partial \hat{r}_1'}+p\frac{\partial G_1}{\partial \hat{r}_1'}\right)\hat{r}_1'-\left(\frac{\partial F_1}{\partial \hat{z}_1'}+p\frac{\partial G_1}{\partial \hat{z}_1'}\right)\hat{z}_1'\right\}\delta R_1\Big|_{R_1=0}^{R_1=A}\ldots\\
&+\left(F_2-\frac{\partial F_2}{\partial \hat{r}_2'}\hat{r}_2'-\frac{\partial F_2}{\partial \hat{z}_2'}\hat{z}_2'\right)\delta R_2\Big|_{R_2=A}^{R_2=R_0}=0,
\end{aligned}\tag{5.5}$$

where the vertical bar '|' signifies evaluation at the boundaries as indicated, e.g.

$$\frac{\partial F}{\partial z'}\delta z\Big|_{r=0}^{r=a}=\frac{\partial F}{\partial z'}(a,z(a),z'(a))\delta z(r(a))-\frac{\partial F}{\partial z'}(0,z(0),z'(0))\delta z(r(0)).\tag{5.6}$$

Now, the perturbations at the boundaries in (5.5) are not arbitrary. Indeed, as discussed above, because of symmetry, $\delta r|_{r=0}=\delta\hat{r}_1|_{R_1=0}=\delta R_1|_{R_1=0}=0$. Further, as the membrane is pinned at $R_2=R_0$, we must have $\delta\hat{r}_2|_{r_2=r_0}=\delta\hat{z}_2|_{R_2=R_0}=\delta R_2|_{R_2=R_0}=0$. Here, we remind ourselves that $z_k(r_k)=\hat{z}_k(R_k)$ with $r_k=\hat{r}_k(R_k)$ for $k=1$ and 2.

The three-phase contact line is the circle defined by $r=a$, the materials points of which lie on the circle $R_1=A=R_2$ in the reference configurations of the wet and dry membranes. At the triple point defined in the rz plane by this contact circle, the profiles of the drop and the wet and dry membranes intersect. Thus, all admissible perturbations in the fields $z(r)$, $\hat{r}_k(R_k)$ and $\hat{z}_k(R_k)$, with $k=1,2$, must satisfy $r=a$, $R_1=R_2=A$, $\hat{r}_1(R_1=A)=\hat{r}_2(R_2=A)=a$ and $z(r=a)=\hat{z}_1(R_1=A)=\hat{z}_2(R_2=A)$, so that

$$\delta r=\delta a,\ \delta R_1=\delta R_2=\delta A,\ \delta\hat{r}_1(A)=\delta\hat{r}_2(A)=\delta a \text{ and } \delta z(a)=\delta\hat{z}_1(A)=\delta\hat{z}_2(A).\tag{5.7}$$

Note that δa denotes δr at $r=a$, i.e. the perturbation in the radial location of the triple point in the current configuration, while δA is the perturbation in the reference location of the contact circle. The two perturbations δa and δA are independent, because they are linked by the membrane's deformation field, which is itself perturbed. Thus, in (5.5) the

perturbations $\delta z(0)$, $\delta\hat{z}_1(0)$, $\delta z(a)$, δa and δA are independent, so that the vanishing of the left-hand side of (5.5) for all admissible perturbations leads to the following boundary conditions:

$$-\left(\frac{\partial F}{\partial z'}+p\frac{\partial G}{\partial z'}\right)\bigg|_0=0, \tag{5.8a}$$

$$-\left(\frac{\partial F_1}{\partial \hat{z}_1'}+p\frac{\partial G_1}{\partial \hat{z}_1'}\right)\bigg|_0=0, \tag{5.8b}$$

$$\left\{(F+pG)-\left(\frac{\partial F}{\partial z'}+p\frac{\partial G}{\partial z'}\right)z'+\left(\frac{\partial F_1}{\partial \hat{r}_1'}+p\frac{\partial G_1}{\partial \hat{r}_1'}\right)-\frac{\partial F_2}{\partial \hat{r}_2'}\right\}\bigg|_{a,A}=0, \tag{5.8c}$$

$$\left\{\left(\frac{\partial F}{\partial z'}+p\frac{\partial G}{\partial z'}\right)+\left(\frac{\partial F_1}{\partial \hat{z}_1'}+p\frac{\partial G_1}{\partial \hat{z}_1'}\right)-\frac{\partial F_2}{\partial \hat{z}_2'}\right\}\bigg|_{a,A}=0 \tag{5.8d}$$

and

$$\left\{(F_1+pG_1)-\left(\frac{\partial F_1}{\partial \hat{r}_1'}+p\frac{\partial G_1}{\partial \hat{r}_1'}\right)\hat{r}_1'\ \ldots\right.$$
$$\left.-\left(\frac{\partial F_1}{\partial \hat{z}_1'}+p\frac{\partial G_1}{\partial \hat{z}_1'}\right)\hat{z}_1'-\left(F_2-\frac{\partial F_2}{\partial \hat{r}_2'}\hat{r}_2'-\frac{\partial F_2}{\partial \hat{z}_2'}\hat{z}_2'\right)\right\}\bigg|_a=0. \tag{5.8e}$$

From (5.8*a*) and (5.8*b*) we may recover the boundary conditions for the drop (2.2*b*) and the wet membrane (2.15*a*). Similarly, from (5.8*c*) and (5.8*d*), we obtain the horizontal (2.14*a*) and vertical (2.14*b*) force balances at the triple point, with $\bar{T}_{wm}=\bar{T}_{s1}$ and $\bar{T}_{dm}=\bar{T}_{s2}$. We note from the sketch in figure 4 that $z'=-j\tan\theta_d$, $z_1'=\tan\theta_{wm}$ and $z_2'=\tan\theta_{dm}$.

Finally, from (5.8*e*) we obtain

$$\left(\frac{W_1}{\hat{\lambda}_{\phi 1}}-T^m_{s1}\hat{\lambda}_{s1}\right)\bigg|_a=\left(\frac{W_2}{\hat{\lambda}_{\phi 2}}-\bar{T}^m_{s2}\hat{\lambda}_{s2}\right)\bigg|_a. \tag{5.9}$$

We recall from (3.2) and (2.11) that the strain energies for an I_2 membrane of the wet and dry parts, and the mechanical tensions in them are, respectively,

$$W_k=\mu t_r\{(\hat{\lambda}_{sk}\hat{\lambda}_{\phi k})^2-3\}\quad\text{and}\quad T^m_{sk}=\hat{\lambda}^{-1}_{\phi k}(\mathrm{d}W_k/\mathrm{d}\hat{\lambda}_{sk}),\quad k=1,2, \tag{5.10a,b}$$

where we have employed the definitions for I_2 and the mechanical tension. From the definitions of the circumferential stretches $\hat{\lambda}_{\phi k}$ and the continuity of $\hat{r}_k$ and r_k at $R_1=R_2=A$, we have

$$\hat{\lambda}_{\phi 1}=\hat{\lambda}_{\phi 2}\quad\text{at } R_1=R_2=A. \tag{5.11}$$

Combining the preceding two equations with (5.9) reduces it to

$$\hat{\lambda}_{s1}=\hat{\lambda}_{s2}\quad\text{at } R_1=R_2=A; \tag{5.12}$$

thus, the meridional stretches in the wet and dry membranes must be continuous at the triple point $r=r_1=r_2=a$. This is the additional condition that was missing in the formulation of § 2.1, which led to a multiplicity of equilibrium solutions in § 4.

An immediate consequence of (5.12) is that the mechanical wet and dry membrane tensions at the triple point are equal, i.e.

$$\bar{T}^m_{wm}=\bar{T}^m_{dm}=\bar{T}^m, \tag{5.13}$$

and, because the wet and dry membrane tensions are uniform in their respective domains, therefore $\bar{T}^m$ is, in fact, the uniform mechanical tension throughout the membrane.

Schulman & Dalnoki-Veress (2015), when modelling their experiments involving micro-droplets on thin, free-standing films, had assumed both a uniform mechanical tension as well as its continuity at the triple point. Here we provide theoretical support to those claims for membranes made of I_2 materials with large stretches.

The revised solution procedure is provided in Appendix C. Returning to the remark at the end of § 3, we now see that the system's equilibrium landscape may be generated by varying only two parameters, which are taken to be the apex drop curvature β and contact circle radius $\bar{a}$ in the above algorithm. However, we prefer to report our results below in terms of the drop volume $\bar{V}$ and the membrane pre-tension $\bar{T}_0$, which are a more natural and practically useful set of control parameters. This may be accomplished by inverting the solutions found utilizing the procedure in Appendix C appropriately.

6. Results and discussion

Before we proceed to present and discuss the results, we reiterate here that the drop equations are solved independently of the membrane underneath. Furthermore, the quantities characterizing the membrane's equilibrium, such as $\bar{z}_k$, $\bar{T}_k$ and θ_k, $k = wm$ or dm, are obtained without the specification of the parameter $\alpha_0 = \mu t_0/\gamma$ – the scaled shear modulus of the membrane. Thus, results that are discussed subsequently depend only upon the scaled interfacial properties of the system, namely $\bar{\gamma}_{sv}$ and $\bar{\gamma}_{sl}$. This does not include the membrane's pre-stretch, which was shown to depend upon α_0 in (3.12).

The values for various system parameters necessary to obtain the results are as follows. We set the parameter $\omega = r_0/l_c = \sqrt{\bar{g}}$ where $\bar{g} = g(l_0^2\rho/\gamma)$ and we set $\bar{g} = 10$. This is consistent with typical experimental values for the system span $r_0 = 0.01$ m, drop density $\rho = 1000\ \mathrm{kg\ m^{-3}}$ and drop surface tension $\gamma = 0.1\ \mathrm{N\ m^{-1}}$. The scaled membrane–air surface tension $\bar{\gamma}_{sv} = 0.5$. Because we take surface energies to be constant, consideration of the equilibrium of the contact line of the drop on a rigid substrate, made up of material that has the same interfacial properties as that of the membrane material, will lead to the relation

$$\bar{\gamma}_{sl} = \bar{\gamma}_{sv} - \cos\theta_{dY}, \tag{6.1}$$

where $\bar{\gamma}_{sl}$ is the scaled membrane–drop surface tension and θ_{dY} is the Young–Dupré equilibrium contact angle (de Gennes *et al.* 2004). We select $\theta_{dY} = 75^\circ$, which is close to $\theta_{dY} = 71 \pm 1^\circ$ made by glycerol on polycarbonate glass (Schulman *et al.* 2018).

6.1. *Equilibrium shapes*

Figure 5 shows the equilibrium configurations of both sessile and pendent drops for several drop volumes. Expectedly, the membrane deforms more with increase in drop volume for sessile drops in figure 5(*a*). For pendent drops in figure 5(*b*), however, the membrane deforms by bulging upwards, with the bulge reducing as the drop volume is raised. The upward bulge in pendent drops has been observed in experiments (Nadermann *et al.* 2013; Schulman & Dalnoki-Veress 2015) and has also been predicted in planar systems (Hui & Jagota 2015; Nair *et al.* 2018). We also note that the dry membrane does not remain flat, and we will return to this point later when we discuss the dry membrane angle in § 6.2.

Pendent drops on rigid substrates are known to exhibit richer behaviour (Thomson 1886) with multiple equilibrium shapes existing for a given volume, all of which are not stable (Wente 1980; Sumesh & Govindarajan 2010; Pozrikidis 2012). Here, for brevity, we do not investigate the possibility of multiple equilibrium shapes in systems with pendent drops.

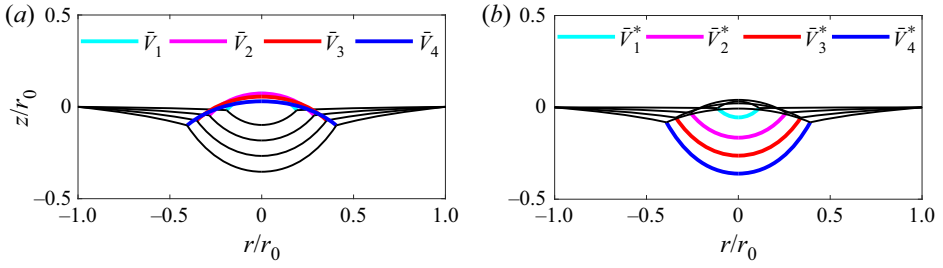

Figure 5. Equilibrium configurations of a pre-stretched nonlinear elastic membrane with (*a*) a sessile drop and (*b*) a pendent drop for several drop volumes: for sessile drops, $\bar{V}_1 < \bar{V}_2 < \bar{V}_3 < \bar{V}_4$, and for pendent drops, $\bar{V}_1^* < \bar{V}_2^* < \bar{V}_3^* < \bar{V}_4^*$, with $\bar{V}_1 = 0.0104$, $\bar{V}_2 = 0.0349$, $\bar{V}_3 = 0.0676$ and $\bar{V}_4 = 0.1063$, while $\bar{V}_1^* = 0.0018$, $\bar{V}_2^* = 0.0231$, $\bar{V}_3^* = 0.0548$ and $\bar{V}_4^* = 0.0911$. The membrane's pre-tension $\bar{T}_0 = 1.5$.

6.2. *Discussion*

We now investigate the effect of drop volume $\bar{V}$, for a fixed membrane pre-tension $\bar{T}_0$, on the following physical quantities: the drop angle θ_d, the wet (θ_{wm}) and dry (θ_{dm}) membrane angles and the wet ($\bar{T}_{wm}$) and dry ($\bar{T}_{dm}$) membrane tensions. We also consider the variation of these quantities with pre-tension $\bar{T}_0$ for a fixed volume V. We recall from the discussion following (3.15) that the pre-tension $\bar{T}_0$ is independent of $\alpha_0 = \mu t_0/\gamma$ and, thus, the results here hold for any membrane material and thickness, as long as the scaled solid surface tensions $\bar{\gamma}_{sv}$ and $\bar{\gamma}_{sl}$ and the parameter $\omega = r_0/l_c$ related to the drop are identical. At the same time, from (3.14) it is clear that membranes with different α_0 must have different unstretched lengths for a fixed system size r_0, in order to have identical pre-tensions.

Figure 6 shows the variation of the angles θ_d, θ_{wm} and θ_{dm} with drop volume $\bar{V}$. First, we note that a negative (positive) wet membrane angle θ_{wm} corresponds to a bulge (sag) in the membrane. As expected, a rise in the drop volume augments the dry membrane angle θ_{dm} monotonically for both sessile drops in figure 6(*a*) and pendent drops in figure 6(*b*). However, both the drop angle θ_d and the wet membrane angle θ_{wm} display contrasting behaviours for sessile and pendent drops. For the former, we observe that the increase in weight of the drop at higher $\bar{V}$ elevates the pressure transferred to the membrane, thereby enlarging θ_{wm}, and correspondingly diminishing θ_d. For pendent drops, in contrast, a rise in the volume increases the weight of the hanging drop and, so, reduces the membrane's upward bulge, thereby lowering the wet membrane angle. The larger volume is accommodated by expanding the drop angle.

We make two additional remarks. First, in the absence of gravity, it is usually assumed that the dry membrane angle θ_{dm} is zero (Davidovitch & Vella 2018; Liu *et al.* 2020). In the present system, however, because we consider gravity, we do not make this assumption and instead calculate θ_{dm}. We find that θ_{dm} in figure 6 deviates significantly from 0°, but becomes smaller when the drop's volume, and hence its weight, shrinks. Thus, except maybe for tiny droplets deforming thin free-standing structures (Schulman & Dalnoki-Veress 2015), assuming that the dry part of the membrane remains flat may not be reasonable. Second, we observe in figure 6 that the wet and dry membrane angles are large in magnitude, thereby necessitating a large-deformation theory when modelling the membrane, as done here.

Figure 7 shows the variation with volume $\bar{V}$ of the wet ($\bar{T}_{wm}$) and dry ($\bar{T}_{dm}$) membrane tensions. For sessile drops in figure 7(*a*), we observe that both $\bar{T}_{wm}$ and $\bar{T}_{dm}$ rise moderately with V, while remaining almost constant for pendent drops in figure 7(*b*). We note, however, that for both sessile and pendent drops, $\bar{T}_{wm}$ is within 15 %–20 % of the

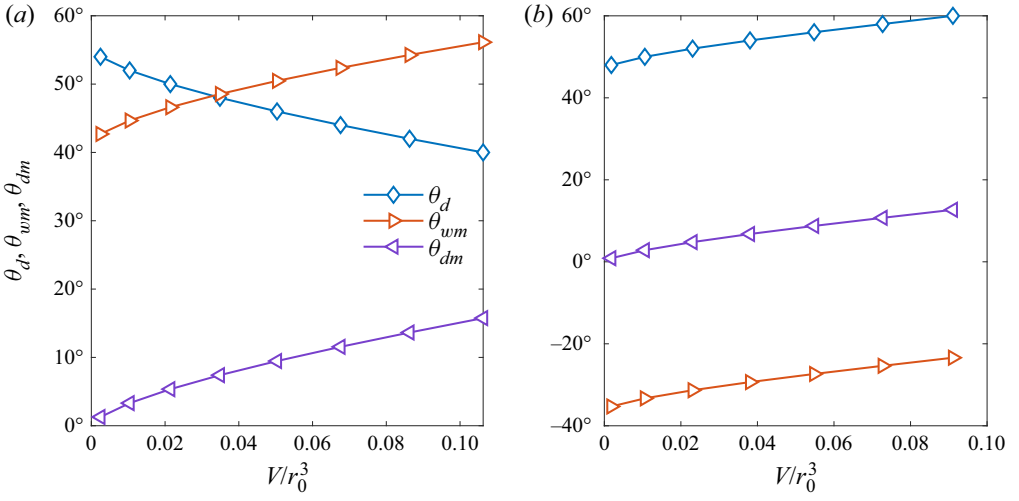

Figure 6. Variation of drop angle θ_d and wet (θ_{wm}) and dry (θ_{dm}) membrane angles with drop volume $\bar{V}$ for (a) a sessile drop and (b) a pendent drop on a pre-stretched nonlinear elastic membrane. The membrane pre-tension $\bar{T}_0 = 1.5$.

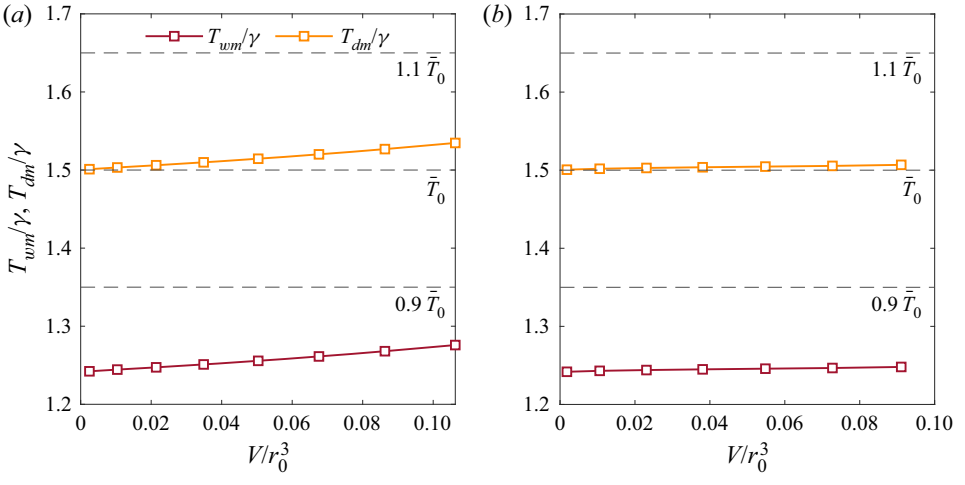

Figure 7. Variation with drop volume $\bar{V}$ of wet ($\bar{T}_{wm}$) and dry ($\bar{T}_{dm}$) membrane tensions for (a) a sessile drop and (b) a pendent drop on a pre-stretched nonlinear elastic membrane. The membrane pre-tension $\bar{T}_0 = 1.5$.

membrane pre-tension $\bar{T}_0$, as may be estimated from the numbers next to the horizontal dashed lines. On the other hand, $\bar{T}_{dm}$ remains always within 1 %–5 % of $\bar{T}_0$. This suggests that, in a practical setting, we may utilize either $\bar{T}_0$ or $\bar{T}_{dm}$ to estimate the other tension to a very good approximation, at least over the range of parameters investigated in figure 7. Even otherwise, the present development relates the membrane pre-tension in a precise way to the current tension field. In this way we overcome a shortcoming pointed out in present models by Davidovitch & Vella (2018, § 5.2): these models are unable to capture the strongly nonlinear response exhibited by the solid in some experiments, preventing them from being employed as elastocapillary probes for pre-tension.

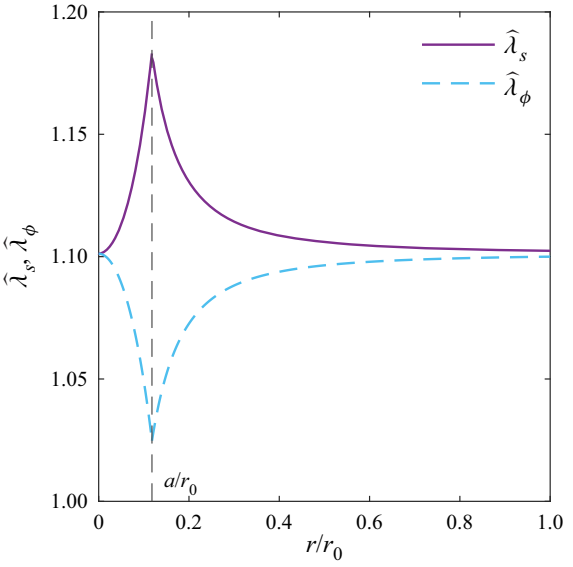

Figure 8. The distribution of total meridional ($\hat{\lambda}_s$) and circumferential ($\hat{\lambda}_\phi$) stretches in the wet and dry regions of the membrane for a sessile drop volume $\bar{V}_0 = 0.0025$ and membrane pre-tension $\bar{T}_0 = 1.5$.

From the definitions of the mechanical tensions and (5.13) we find that $\bar{T}_{dm} - \bar{T}_{wm} = \gamma_{sv} - \gamma_{sl} = \cos\theta_{dY}$, where θ_{dY} is the Young–Dupré equilibrium contact angle. Because we have set $\theta_{dY} = 75^\circ$, $\bar{T}_{wm} > \bar{T}_{dm}$ in figure 7. In contrast, for $\theta_{dY} \geq 90^\circ$, we would have had $\bar{T}_{wm} \geq \bar{T}_{dm}$ with $\bar{T}_{dm}$ being still within 1 %–5 % of $\bar{T}_0$.

Figure 8 reports the distribution of total meridional and circumferential stretches in the membrane for a sessile drop. For practical values of drop volume and membrane pre-tension, we observe that the stretches are appreciable, and they may be as large as 15 % near the triple point. This further supports the need to develop a large-deformation theory to model elastocapillary systems involving thin solids.

In figure 9, we report the effect of the membrane pre-tension $\bar{T}_0$ upon the membrane tensions and the drop and membrane angles for a fixed drop volume $\bar{V}$. We restrict to a sessile drop. We observe in figure 9(*a*) that the wet membrane tension $\bar{T}_{wm}$ is closer to $\bar{T}_0$ at higher pre-tension. In addition, we find from figure 9(*b*) that as $\bar{T}_0$ is increased, the drop angle θ_d tends to the Young–Dupré equilibrium angle θ_{dY} for a substrate whose surface properties are identical to those of the membrane material; recall that in our case $\theta_{dY} = 75^\circ$. Moreover, both the membrane angles, θ_{wm} and θ_{dm}, approach 0° with increase in $\bar{T}_0$. In this way, we recover the rigid substrate solution at high pre-tension.

The inset in figure 9(*b*) shows the variation of the angles θ_d, θ_{wm} and θ_{dm} with the wet membrane tension $\bar{T}_{wm}$. We note that at lower $\bar{T}_{wm}$, we have $\theta_{wm} > \theta_d$. This is in contrast with the experiments of Schulman & Dalnoki-Veress (2015), who studied micro-droplets on deformable free-standing films, where $\theta_d > \theta_{wm}$ was claimed for all wet membrane tensions. A possible explanation of this could be that experiments had micro-drops with dimensional volumes of about 0.015 µl, for which gravity effects could be ignored and the dry membrane was reported to be flat within 1.5°. Indeed, in the inset of figure 9(*b*), we set the drop's volume $\bar{V}_0 = 0.05$ (about 50 µl) and gravity effects are sufficient to cause the dry membrane to deviate up to 10° at low tensions, where changes in θ_d and θ_{wm} are rapid. At the same time, we observe a very good match when we compare in figure 9(*c*) our

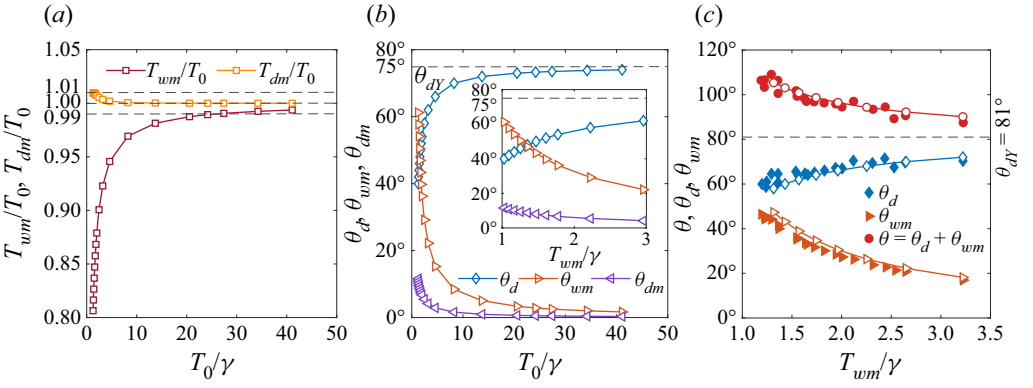

Figure 9. Variation with membrane pre-tension $\bar{T}_0$ of (*a*) wet ($\bar{T}_{wm}$) and dry ($\bar{T}_{dm}$) membrane tensions, and (*b*) drop angle θ_d, and wet (θ_{wm}) and dry (θ_{dm}) membrane angles for a sessile drop placed upon a pre-stretched nonlinear elastic membrane. Inset in (*b*) plots θ_d, θ_{wm} and θ_{dm} against $\bar{T}_{wm}$. The drop volume $\bar{V} = 0.05$. (*c*) Comparison of our predictions (solid curves) with experiments of Schulman & Dalnoki-Veress (2015).

predictions directly with experiments of Schulman & Dalnoki-Veress (2015) with glycerol micro-droplets on free-standing elastomeric films made of styrene–isoprene–styrene.

We now make some remarks about the recent experiments of Kumar *et al.* (2020), who claim that the tension in an elastic film in contact with a liquid is determined only by the liquid's surface tension and is unaffected by solid surface energies. Their experimental system consisted of a thin elastic film that was first floated on a liquid bath and then partially lifted up vertically from one end. This then formed a three-phase contact point where the vertical part of the film met with the free surface of the liquid and the part of the film still resting upon the liquid. Because the shapes of the liquid's free surface and that of the film in contact with the liquid were identical, this showed that that tension in the film equals the the liquid–vapour interfacial tension, irrespective of the solid's surface properties.

The above result of Kumar *et al.* (2020) may lead to the impression that elastocapillary systems, like the one we investigate, cannot be utilized to measure solid surface properties. The present investigation, however, permits us to make two important clarifications that counter this impression. First, the tension in the film that Kumar *et al.* (2020) discuss is really the total tension comprising the mechanical tension and the contributions of the solid's surface interactions; recall figure 1(*c*), relation (2.6) and associated discussion. Thus, even if the total tension remains constant, the mechanical tension will change if the solid's surface properties are varied, and this will be reflected in the film's stretches. Next, the total tension remains the same in the experiments of Kumar *et al.* (2020) because of the simple geometry involved, and this will not be true for more complex systems as we show below.

To study the effect of solid surface tension, we set $\gamma_{sv} = 0$ and report in figure 10 the changes in the contact angles, the membrane tensions and the contact radius as we vary γ_{sl}/γ. We observe from figure 10(*a*) that the variation in drop and membrane angles is significant. In particular, the drop angle θ_d changes by as much as 40° when γ_{sl}/γ is raised from 0 to 0.75. The corresponding deviations in the wet (θ_{wm}) and dry (θ_{dm}) membrane angles at low values of pre-tension are, respectively, 10°–15° and 2°–3°. Similarly, in figure 10(*b*), we find that the departures in the wet ($\bar{T}_{wm}$) tension may be nearly 40 %; the curve for $\gamma_{sl}/\gamma = 0$ lies on top of the curve for dry membrane tension ($\bar{T}_{dm}$).

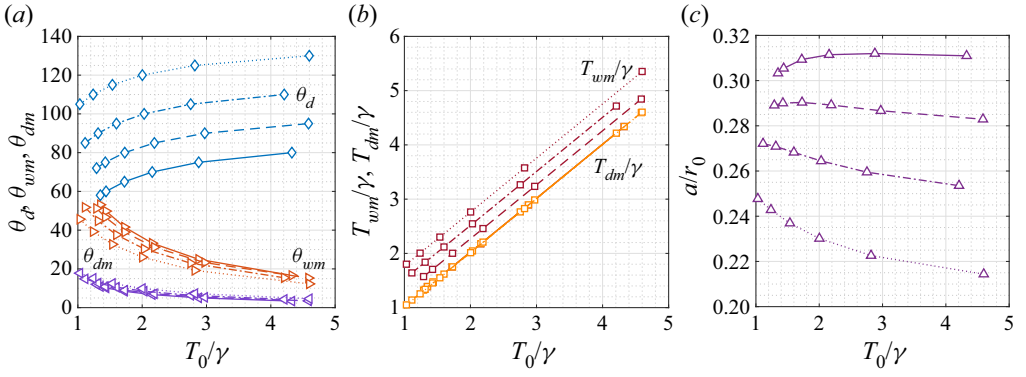

Figure 10. Variation with membrane pre-tension $\bar{T}_0$ of (a) drop angle θ_d and wet (θ_{wm}) and dry (θ_{dm}) membrane angles, (b) the wet ($\bar{T}_{wm}$) and dry ($\bar{T}_{dm}$) membrane tensions and (c) contact radius $\bar{a}$. Several values of γ_{sl}/γ are considered: 0 (solid), 0.25 (dashed), 0.5 (dashed-dot) and 0.75 (dotted). The drop volume $\bar{V} = 0.05$ and surface tension $\gamma_{sv} = 0$.

The dry membrane tension remained identical as $\gamma_{sv} = 0$ was fixed, and we note here that the important parameter to track is the difference in the solid surface tensions $\gamma_{sl} - \gamma_{sv}$. Finally, figure 10($c$) shows that the contact circle is also modified appreciably. These results demonstrate that the solid's surface properties introduce measurable adjustments in elastocapillary systems, such as the one in figure 1.

We end this section with a potential application of the theory to measure solid surface energies. We perform two experiments, one each at high and low pre-tension T_0. This may be accomplished in the same experimental setup by taking two different sized unstretched membranes, one small and one large. At high T_0, as figure 9(b) shows, we obtain θ_{dY} by measuring the drop angle θ_d. This then allows us to relate the surface energies through (6.1), assuming them to be constant. Another relation between the surface energies γ_{sv} and γ_{sl} may be obtained from the experiment at low T_0 by combining (3.14), (3.15), the definitions of the mechanical tensions $\bar{T}^m_{wm}$ and $\bar{T}^m_{dm}$, (3.3) and (3.4). The surface energies γ_{sv} and γ_{sl} may now be calculated.

7. Conclusions

In this work, we have reported the axisymmetric equilibrium shapes of a system consisting of a nonlinear pre-stretched elastic membrane with sessile or pendent drops. For simplicity we considered I_2 membranes, i.e. membranes made of hyperelastic materials whose response is dominated by the second stress invariant I_2. In such membranes, the mechanical tension was shown to be equibiaxial. This facilitated the direct computation of the system's equilibrium state without requiring recourse to the membrane's reference configuration. Subsequently, we obtained a closed-form solution for membrane pre-tension corresponding to the given equilibrium configuration.

We then showed that balance of forces alone yielded non-unique equilibrium solutions for a given drop liquid and volume, membrane type and pre-tension, contrary to expectations and available observations. To find the missing conditions, if any, that would make the equilibrium solution unique, we then postulated that the system's equilibrium coincided with the minimum of its potential energy. Because the membrane's undeformed extent and the drop's volume are kept constant while minimizing the potential energy,

this process was equivalent to minimizing the system's Helmholtz free energy. Through this we uncovered an additional necessary condition characterizing the equilibrium: the continuity of meridional stretches across the three-phase contact line. The equilibrium was then found to be unique.

We subsequently investigated the effects of the drop volume and the membrane pre-tension on the tensions in the membrane's wet and dry parts, and the angles made with the horizontal at the triple point by the drop and the wet and dry membranes at equilibrium. We demonstrated that the pre-tension in the membrane could be employed to estimate the dry and wet membrane tensions to a good approximation, which provides an alternative way for the mechanical characterization of thin sheets. Furthermore, our results are independent of the membrane's shear modulus and thickness, and depend only upon the parameter $\omega = r_0/l_c$, where l_c is capillary length of the drop's liquid and r_0 is the system's span, and the energies at the liquid–air, membrane–air and membrane–liquid interfaces.

Finally, we made contact with the recent works of Davidovitch & Vella (2018) and Kumar *et al.* (2020). We demonstrated how utilizing a large-deformation analysis for the membrane enabled us to relate the pre-tension in the membrane to its current tension. This then allows us to employ drops as elastocapillary probes to estimate membrane pre-tension. We then established consistency of our development with the experiments of Kumar *et al.* (2020) and, in the process, clarified the implications of their results. Further, utilizing the system of figure 1 we illustrated how solid surface properties may indeed measurably modify an elastocapillary system's equilibrium, including the stress state in the solid. Based on this we suggested a protocol by which we may characterize thin elastic structures – specifically their surface energies – through their interactions with drops.

Acknowledgements. We thank all three reviewers for their comments that greatly improved the manuscript. V.N. thanks the Ministry of Education, Government of India, for financial support during his PhD. We also thank Prof. Anindya Chatterjee, Prof. Anurag Gupta and Prof. Chandra Shekhar Upadhyay of IIT Kanpur for helpful discussions.

Funding. This research received no specific grant.

Declaration of interests. The authors report no conflict of interest.

Author ORCIDs.
Vineet Nair https://orcid.org/0000-0001-5351-9840;
Ishan Sharma https://orcid.org/0000-0002-8447-4857;
V. Shankar https://orcid.org/0000-0003-0233-7494.

Appendix A. Alternative derivation of the membrane's governing equations

We outline how the governing equations in § 2 for a membrane with active surface tensions may be obtained from the full three-dimensional elasticity equations by averaging. The free-body diagram of an element of a membrane is shown in figure 11. In a force-based formulation the effect of surface energies is assumed to be captured by surface tensions applied at the edges of the membrane.

The vector sum of forces acting on a membrane element is

$$\int_{-h/2}^{h/2} (\sigma_{tt} r \hat{\boldsymbol{e}}_t)|_{s+\Delta s} \Delta\phi \, \mathrm{d}z - \int_{-h/2}^{h/2} (\sigma_{tt} r \hat{\boldsymbol{e}}_t)|_{s} \Delta\phi \, \mathrm{d}z + \int_{-h/2}^{h/2} (\sigma_{\phi\phi} \hat{\boldsymbol{e}}_\phi)|_{\phi+\Delta\phi} \Delta s \, \mathrm{d}z \ldots$$

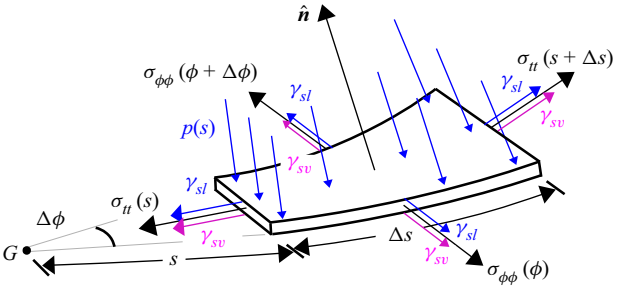

Figure 11. Free-body diagram of a membrane element with normal $\hat{\boldsymbol{n}}$ at equilibrium. The other quantities are defined in the caption to figure 1 and the associated text.

$$-\int_{-h/2}^{h/2}(\sigma_{\phi\phi}\hat{\boldsymbol{e}}_\phi)|_\phi\,\Delta s\,\mathrm{d}z+\boldsymbol{f}r\Delta s\Delta\phi+\{(\gamma_{sl}+\gamma_{sv})r\hat{\boldsymbol{e}}_t\}|_{s+\Delta s}\Delta\phi\ldots$$
$$-\{(\gamma_{sl}+\gamma_{sv})r\hat{\boldsymbol{e}}_t\}|_s\Delta\phi+\{(\gamma_{sl}+\gamma_{sv})\hat{\boldsymbol{e}}_\phi\}|_{\phi+\Delta\phi}\Delta s-\{(\gamma_{sl}+\gamma_{sv})\hat{\boldsymbol{e}}_\phi\}|_\phi\Delta s=0,\quad\text{(A1)}$$

where $\boldsymbol{f}=-p\hat{\boldsymbol{n}}$ is the pressure acting on the membrane and the vertical bar '|' signifies evaluation at the specified point, e.g. $(\sigma_{tt}r\hat{\boldsymbol{e}}_t)|_{s+\Delta s}=\sigma_{tt}(s+\Delta s)r(s+\Delta s)\hat{\boldsymbol{e}}_t(s+\Delta s)$. We rewrite the above force balance to obtain

$$(\bar{\sigma}_{tt}r\hat{\boldsymbol{e}}_t)|_{s+\Delta s}\Delta\phi-(\bar{\sigma}_{tt}r\hat{\boldsymbol{e}}_t)|_s\Delta\phi+(\bar{\sigma}_{\phi\phi}\hat{\boldsymbol{e}}_\phi)|_{\phi+\Delta\phi}\Delta s-(\bar{\sigma}_{\phi\phi}\hat{\boldsymbol{e}}_\phi)|_\phi\Delta s\ldots$$
$$+\boldsymbol{f}r\Delta s\Delta\phi+\{(\gamma_{sl}+\gamma_{sv})r\hat{\boldsymbol{e}}_t\}|_{s+\Delta s}\Delta\phi-\{(\gamma_{sl}+\gamma_{sv})r\hat{\boldsymbol{e}}_t\}|_s\Delta\phi\ldots$$
$$+\{(\gamma_{sl}+\gamma_{sv})\hat{\boldsymbol{e}}_\phi\}|_{\phi+\Delta\phi}\Delta s-\{(\gamma_{sl}+\gamma_{sv})\hat{\boldsymbol{e}}_\phi\}|_\phi\Delta s=0,\quad\text{(A2)}$$

where quantities with an overbar are depth-averaged (thickness-averaged) quantities, e.g.

$$\bar{\sigma}_{tt}|_{s+\Delta s}=\int_{-h/2}^{h/2}\sigma_{tt}|_{s+\Delta s}\,\mathrm{d}z.\quad\text{(A3)}$$

Dividing (A2) by $\Delta s\Delta\phi$ and taking the limit $\Delta s\to 0$ and $\Delta\phi\to 0$, we obtain

$$\frac{\partial\{(\bar{\sigma}_{tt}+\gamma_{sl}+\gamma_{sv})r\hat{\boldsymbol{e}}_t\}}{\partial s}+\frac{\partial\{(\bar{\sigma}_{\phi\phi}+\gamma_{sl}+\gamma_{sv})\hat{\boldsymbol{e}}_\phi\}}{\partial\phi}+r\boldsymbol{f}=0.\quad\text{(A4)}$$

We now set

$$T_s=\bar{\sigma}_{tt}+\gamma_{sl}+\gamma_{sv}\quad\text{and}\quad T_\phi=\bar{\sigma}_{\phi\phi}+\gamma_{sl}+\gamma_{sv},\quad\text{(A5}a,b\text{)}$$

where we recognize the depth-averaged Cauchy stresses $\bar{\sigma}_{tt}$ and $\bar{\sigma}_{\phi\phi}$ as the *mechanical* tensions T_s^m and T_ϕ^m. The above matches (2.6) showing that averaging automatically combines depth-averaged Cauchy stress (mechanical tensions) with surface tensions.

Now, we also have the relations

$$\hat{\boldsymbol{e}}_t=\cos\theta\hat{\boldsymbol{e}}_r+\sin\theta\hat{\boldsymbol{e}}_z,\quad\hat{\boldsymbol{n}}=-\sin\theta\hat{\boldsymbol{e}}_r+\cos\theta\hat{\boldsymbol{e}}_z,\quad\text{(A6}a\text{)}$$

$$\frac{\partial\hat{\boldsymbol{e}}_t}{\partial s}=\frac{\mathrm{d}\theta}{\mathrm{d}s}\hat{\boldsymbol{n}},\quad\frac{\partial\hat{\boldsymbol{e}}_\phi}{\partial\phi}=-\cos\theta\hat{\boldsymbol{e}}_t+\sin\theta\hat{\boldsymbol{n}}\quad\text{and}\quad\frac{\partial r}{\partial s}=\cos\theta.\quad\text{(A6}b\text{)}$$

Combining (A5) and (A6) with (A4) we may express the mechanical equilibrium of the membrane's element by

$$\left(T_s\cos\theta+r\frac{\partial T_s}{\partial s}-T_\phi\cos\theta\right)\hat{\boldsymbol{e}}_t+\left(rT_s\frac{\mathrm{d}\theta}{\mathrm{d}s}+T_\phi\sin\theta-rp\right)\hat{\boldsymbol{n}}+\frac{\partial T_\phi}{\partial\phi}\hat{\boldsymbol{e}}_\phi=0.\quad\text{(A7)}$$

From the above we obtain three scalar equations in the $\hat{\boldsymbol{e}}_\phi$, $\hat{\boldsymbol{e}}_t$ and $\hat{\boldsymbol{n}}$ directions, respectively,

$$\frac{\partial T_\phi}{\partial \phi} = 0, \tag{A8a}$$

$$\frac{\partial T_s}{\partial s} = \frac{(T_\phi - T_s)\cos\theta}{r} \iff \frac{\partial T_s}{\partial r} = \frac{(T_\phi - T_s)}{r}, \tag{A8b}$$

and

$$\kappa_s T_s + \kappa_\phi T_\phi = p, \tag{A8c}$$

where $\kappa_s = \mathrm{d}\theta/\mathrm{d}s$ and $\kappa_\phi = \sin\theta/r$ are the principal curvatures of the membrane in its equilibrium configuration (DoCarmo 2016). While (A8*a*) expresses the axisymmetric nature of the system, (A8*b*) and (A8*c*) recover (2.3). Combined with (A5) we see that it is the *total* tension that governs the membrane's deformation, where the total tensions are comprised of mechanical tensions (depth-averaged Cauchy stress) and surface tensions.

Appendix B. Solution procedure

We provide below an outline of our solution procedure.

Step I. For a choice of non-dimensional apex curvature of the drop β and contact radius $\bar{a}$, the governing equation (2.19) for the drop together with the end conditions (2.20) is numerically solved to obtain the drop's profile $\bar{z}_d(\bar{r}_d)$ and, thereby, the drop angle θ_d. We follow the algorithm of Nair *et al.* (2018) to compute shapes when $\bar{z}_d$ is not a single-valued function of $\bar{r}_d$, such as for sessile drops when $\theta_d > 90^\circ$.

Step II. Next, for the drop apex curvature β and contact radius $\bar{a}$ utilized in Step I, the governing equation for the wet membrane (2.23) with boundary conditions (2.24) is solved numerically for different choices of wet membrane tension $\bar{T}_{wm}$ to obtain the profile of the wet membrane $\bar{z}_{wm}(\bar{r}_{wm})$ and the wet membrane angle θ_{wm}.

Step III. Turning to the dry membrane, for θ_d and θ_{wm} found above for a choice of β, $\bar{a}$, and $\bar{T}_{wm}$, we solve (2.27) to obtain the dry membrane tension $\bar{T}_{dm}$ and the dry membrane angle θ_{dm}:

$$\bar{T}_{dm} = \sqrt{\bar{T}_{wm}^2 + 1 + 2\bar{T}_{wm}\cos\theta} \tag{B1}$$

and

$$\theta_{dm} = \theta_{wm} - j\arccos\left(\frac{\bar{T}_{wm}^2 + \bar{T}_{dm}^2 - 1}{2\bar{T}_{wm}\bar{T}_{dm}}\right), \tag{B2}$$

where $\theta = \theta_d + j\theta_{wm}$ is the internal angle made by the drop with the membrane at the triple point and we recall that $j = \pm 1$ for sessile/pendent drops.

Step IV. The non-dimensional profile $\bar{z}_{dm}(\bar{r}_{dm})$ of the dry membrane may now be obtained in closed form by solving (2.25) and (2.26):

$$\bar{z}_{dm} = \bar{a}\sin\theta_{dm}\left\{\operatorname{arccosh}\left(\frac{\bar{r}_{dm}}{\bar{a}\sin\theta_{dm}}\right) - \operatorname{arccosh}\left(\frac{1}{\sin\theta_{dm}}\right)\right\} + \bar{z}_d(\bar{a}), \tag{B3}$$

where $\bar{z}_d(\bar{a})$ is available from Step I.

Step V. Finally, the non-dimensional volume of the drop is computed by utilizing the solutions for the equilibrium shape of the drop and the wet membrane:

$$\bar{V} = 2\pi j \int_0^{\bar{a}} \bar{r}_d \bar{z}_d \, \mathrm{d}\bar{r}_d - 2\pi j \int_0^{\bar{a}} \bar{r}_{wm} \bar{z}_{wm} \, \mathrm{d}\bar{r}_{wm}. \tag{B4}$$

The above procedure is repeated for different combinations of β, $\bar{a}$ and $\bar{T}_{wm}$ to generate the entire range of solutions.

Appendix C. Solution procedure, revised

We now revise our solution procedure outlined in Appendix B to incorporate the extra condition (5.12) at the triple point. As before, for a choice of apex drop curvature β and contact circle's radius $\bar{a}$, we solve (2.19) and (2.20) to obtain the drop's profile $\bar{z}_d(\bar{r}_d)$ and, so, the drop angle θ_d.

Invoking (5.13), we solve (2.27) to express θ_{wm} and θ_{dm} in terms of θ_d:

$$\theta_{wm} = -j\theta_d + \arccos\left\{\frac{\bar{T}_{dm}^2 - \bar{T}_{wm}^2 - 1}{2\bar{T}_{wm}}\right\} \tag{C1a}$$

and

$$\theta_{dm} = -j\theta_d + \arccos\left\{\frac{\bar{T}_{dm}^2 + 1 - \bar{T}_{wm}^2}{2\bar{T}_{dm}}\right\}, \tag{C1b}$$

where $\bar{T}_{wm} = \bar{T}^m + \bar{\gamma}_{sl} + \bar{\gamma}_{sv}$ and $\bar{T}_{dm} = \bar{T}^m + 2\bar{\gamma}_{sv}$, as before. Then, for the chosen β and $\bar{a}$, we solve (2.23) together with (2.24) and (C1a) to obtain the wet membrane profile $\bar{z}_{wm}(\bar{r}_{wm})$ and tension $\bar{T}^m$. Subsequently, we find membrane angles θ_{wm} and θ_{dm}, and membrane tensions $\bar{T}_{wm}$ and $\bar{T}_{dm}$. We note that the additional condition (C1a) has helped us determine $\bar{T}_{wm}$ as part of the solution to the wet membrane's equilibrium whereas, previously, $\bar{T}_{wm}$ was an additional parameter to be specified.

The profile of the dry membrane $\bar{z}_{dm}$, the drop volume $\bar{V}$ and the membrane pre-tension $\bar{T}_0$ are computed as in Appendix B and are given by, respectively, (B3), (B4) and (3.15). This solution procedure is repeated for different combinations of β and $\bar{a}$ to produce the entire range of possible equilibria.

References

Andreotti, B. & Snoeijer, J.H. 2020 Statics and dynamics of soft wetting. *Annu. Rev. Fluid Mech.* **52**, 285–308.

Bashforth, F. & Adams, J.C. 1883 *An Attempt to Test the Theories of Capillary Action: By Comparing the Theoretical and Measured Forms of Drops of Fluid*. Cambridge University Press.

Bico, J., Reyssat, É. & Roman, B. 2018 Elastocapillarity: when surface tension deforms elastic solids. *Annu. Rev. Fluid Mech.* **50**, 629–659.

Davidovitch, B. & Vella, D. 2018 Partial wetting of thin solid sheets under tension. *Soft Matter* **14** (24), 4913–4934.

DoCarmo, M.P. 2016 *Differential Geometry of Curves and Surfaces*. Dover Publications.

Fortes, M.A. 1984 Deformation of solid surfaces due to capillary forces. *J. Colloid Interface Sci.* **100** (1), 17–26.

Gelfand, I.M. & Fomin, S.V. 2000 *Calculus of Variations*. Dover Publications.

de Gennes, P.G., Brochard-Wyart, F. & Quéré, D. 2004 *Capillarity and Wetting Phenomena: Drops, Bubbles, Pearls, Waves*. Springer.

GREEN, A.E. & ADKINS, J.E. 1960 *Large Elastic Deformations and Non-linear Continuum Mechanics*. Clarendon.

HAUGHTON, D.M. 2001 Elastic membranes. In *Nonlinear Elasticity: Theory and Applications* (ed. Y. Fu & R.W. Ogden), pp. 241–242. Cambridge University Press.

HOLZAPFEL, G.A. 2000 *Nonlinear Solid Mechanics. A Continuum Approach for Engineering*, p. 238. John Wiley & Sons.

HUI, C.-Y. & JAGOTA, A. 2015 Planar equilibrium shapes of a liquid drop on a membrane. *Soft Matter* **11** (46), 8960–8967.

KERN, R. & MÜLLER, P. 1992 Deformation of an elastic thin solid induced by a liquid droplet. *Surf. Sci.* **264** (3), 467–494.

KÜHNEL, W. 2015 *Differential Geometry: Curves–Surfaces–Manifolds*. American Mathematical Society.

KUMAR, D., RUSSELL, T.P., DAVIDOVITCH, B. & MENON, N. 2020 Stresses in thin sheets at fluid interfaces. *Nat. Mater.* **19** (7), 690–693.

LESTER, G.R. 1961 Contact angles of liquids at deformable solid surfaces. *J. Colloid Sci.* **16** (4), 315–326.

LIU, T., LIU, Z., JAGOTA, A. & HUI, C.-Y. 2020 Droplets on an elastic membrane: configurational energy balance and modified Young equation. *J. Mech. Phys. Solids* **138**, 103902.

LONG, R. & HUI, C.-Y. 2012 Axisymmetric membrane in adhesive contact with rigid substrates: analytical solutions under large deformation. *Intl J. Solids Struct.* **49** (3–4), 672–683.

LONG, R., SHULL, K.R. & HUI, C.-Y. 2010 Large deformation adhesive contact mechanics of circular membranes with a flat rigid substrate. *J. Mech. Phys. Solids* **58** (9), 1225–1242.

LOVE, A.E.H. 1927 *A Treatise on the Mathematical Theory of Elasticity*. Cambridge University Press.

NADERMANN, N., HUI, C.-Y. & JAGOTA, A. 2013 Solid surface tension measured by a liquid drop under a solid film. *Proc. Natl Acad. Sci.* **110** (26), 10541–10545.

NAIR, V. 2022 Elastocapillarity: equilibrium shapes of drops on thin sheets. PhD thesis, Indian Institute of Technology Kanpur, Kanpur, Uttar Pradesh.

NAIR, V., SHARMA, I. & SHANKAR, V. 2018 Planar equilibria of sessile and pendant liquid drops on geometrically non-linear elastic membranes. *Phys. Fluids* **30** (8), 082114.

NEUKIRCH, S., ANTKOWIAK, A. & MARIGO, J.-J. 2013 The bending of an elastic beam by a liquid drop: a variational approach. *Proc. R. Soc.* A **469** (2157), 20130066.

NEUKIRCH, S., ANTKOWIAK, A. & MARIGO, J.-J. 2014 Soft beams: when capillarity induces axial compression. *Phys. Rev.* E **89** (1), 012401.

OGDEN, R.W. 1997 *Non-linear Elastic Deformations*. Dover.

OLIVES, J. 1993 Capillarity and elasticity. The example of the thin plate. *J. Phys.: Condens. Matter* **5** (14), 2081–2094.

OLIVES, J. 1996 A combined capillarity and elasticity problem for a thin plate. *SIAM J. Appl. Math.* **56** (2), 480–493.

PAULSEN, J.D. 2019 Wrapping liquids, solids, and gases in thin sheets. *Annu. Rev. Condens. Matter Phys.* **10**, 431–450.

POZRIKIDIS, C. 2012 Stability of sessile and pendant liquid drops. *J. Engng Maths* **72**, 1–20.

REDDY, J.N. 2006 *Theory and Analysis of Elastic Plates and Shells*. CRC.

ROMAN, B. & BICO, J. 2010 Elasto-capillarity: deforming an elastic structure with a liquid droplet. *J. Phys.: Condens. Matter* **22** (49), 493101.

RUSANOV, A.I. 1975 Theory of wetting of elastically deformed bodies. 1. Deformation with a finite contact-angle. *Colloid J. USSR* **37** (4), 614–622.

SCHROLL, R.D., ADDA-BEDIA, M., CERDA, E., HUANG, J., MENON, N., RUSSELL, T.P., TOGA, K.B., VELLA, D. & DAVIDOVITCH, B. 2013 Capillary deformations of bendable films. *Phys. Rev. Lett.* **111** (1), 014301.

SCHULMAN, R.D. & DALNOKI-VERESS, K. 2015 Liquid droplets on a highly deformable membrane. *Phys. Rev. Lett.* **115** (20), 206101.

SCHULMAN, R.D., LEDESMA-ALONSO, R., SALEZ, T., RAPHAËL, E. & DALNOKI-VERESS, K. 2017 Liquid droplets act as 'compass needles' for the stresses in a deformable membrane. *Phys. Rev. Lett.* **118** (19), 198002.

SCHULMAN, R.D., TREJO, M., SALEZ, T., RAPHAËL, E. & DALNOKI-VERESS, K. 2018 Surface energy of strained amorphous solids. *Nat. Commun.* **9**, 982.

SHANAHAN, M.E.R. 1985 Contact angle equilibrium on thin elastic solids. *J. Adhes.* **18**, 247–267.

SHANAHAN, M.E.R. 1987 Equilibrium of liquid drops on thin plates; plate rigidity and stability considerations. *J. Adhes.* **20**, 261–274.

SHUTTLEWORTH, R. 1950 The surface tension of solids. *Proc. Phys. Soc.* A **63** (5), 444–457.

STYLE, R.W., JAGOTA, A., HUI, C.-Y. & DUFRESNE, E.R. 2017 Elastocapillarity: surface tension and the mechanics of soft solids. *Annu. Rev. Condens. Matter Phys.* **8**, 99–118.

SUMESH, P.T. & GOVINDARAJAN, R. 2010 The possible equilibrium shapes of static pendant drops. *J. Chem. Phys.* **133** (14), 144707.

THOMSON, W. 1886 Capillary attraction. *Nature* **34**, 290–294.

WENTE, H. 1980 The stability of the axially symmetric pendent drop. *Pac. J. Maths* **88** (2), 421–470.